Uncertainties in eddy covariance air-sea CO_2 flux measurements and implications for gas transfer velocity parameterisations

Yuanxu Dong[1,2], Mingxi Yang[2], Dorothee C. E. Bakker[1], Vassilis Kitidis[2] and Thomas G. Bell[2]

[1]Centre for Ocean and Atmospheric Sciences, School of Environmental Sciences, University of East Anglia, Norwich, UK

[2]Plymouth Marine Laboratory, Prospect Place, Plymouth, UK

Correspondence to: Yuanxu Dong (Yuanxu.Dong@uea.ac.uk)

Abstract. Air-sea carbon dioxide (CO_2) flux is often indirectly estimated by the bulk method using the air-sea difference in CO_2 fugacity ($\Delta f CO_2$) and a parameterisation of the gas transfer velocity (K). Direct flux measurements by eddy covariance (EC) provide an independent reference for bulk flux estimates and are often used to study processes that drive K. However, inherent uncertainties in EC air-sea CO_2 flux measurements from ships have not been well quantified and may confound analyses of K. This paper evaluates the uncertainties in EC CO_2 fluxes from four cruises. Fluxes were measured with two state-of-the-art closed-path CO_2 analysers on two ships. The mean bias in the EC CO_2 flux is low but the random error is relatively large over short time scales. The uncertainty (1 standard deviation) in hourly averaged EC air-sea CO_2 fluxes (cruise-mean) ranges from 1.4 to 3.2 mmol m^{-2} day^{-1}. This corresponds to a relative uncertainty of ~20% during two Arctic cruises that observed large CO_2 flux magnitude. The relative uncertainty was greater (~50%) when the CO_2 flux magnitude was small during two Atlantic cruises. Random uncertainty in the EC CO_2 flux is mostly caused by sampling error. Instrument noise is relatively unimportant. Random uncertainty in EC CO_2 fluxes can be reduced by averaging for longer. However, averaging for too long will result in the inclusion of more natural variability. Auto-covariance analysis of CO_2 fluxes suggests that the optimal timescale for averaging EC CO_2 flux measurements ranges from 1–3 hours, which increases the mean signal-to-noise ratio of the four cruises to higher than 3. Applying an appropriate averaging timescale and suitable $\Delta f CO_2$ threshold (20 µatm) to EC flux data enables an optimal analysis of K.

1 Introduction

Since the Industrial Revolution, atmospheric CO_2 levels have risen steeply due to human activities (Broecker and Peng, 1993). The ocean plays a key role in the global carbon cycle, having taken up roughly one quarter of anthropogenic CO_2 emissions over the last decade (Friedlingstein et al., 2020). Accurate estimates of air-sea CO_2 flux are vital to forecast climate change and to quantify the effects of ocean CO_2 uptake on the marine biosphere.

Air-sea CO_2 flux (F, e.g. in mmol m^{-2} day^{-1}) is typically estimated indirectly by the bulk equation:

$$F = K_{660}(Sc/660)^{-0.5}\, \alpha\left(fCO_{2w} - fCO_{2a}\right) \tag{1}$$

Where K_{660} (in cm h^{-1}) is the gas transfer velocity, usually parameterised as a function of wind speed (e.g. Nightingale et al., 2000), Sc (dimensionless) is the Schmidt number (Wanninkhof, 2014) and α (mol L^{-1} atm^{-1}) is the solubility (Weiss, 1974). Sc is equal to 660 for CO_2 at 20℃ and 35‰ salt water (Wanninkhof et al., 2009). fCO_{2w} and fCO_{2a} are the CO_2 fugacity (in μatm) at the sea surface and in the overlying atmosphere, respectively, with $fCO_{2w} - fCO_{2a}$ the air-sea CO_2 fugacity difference (ΔfCO_2). Uncertainties in the K_{660} parameterisation and limited coverage of fCO_{2w} measurements result in considerable uncertainties in global bulk flux estimates (Takahashi et al., 2009; Woolf et al., 2019).

Eddy covariance (EC) is the most direct method for measuring the air-sea CO_2 flux F:

$$F = \rho\,\overline{w'c'} \tag{2}$$

where ρ is the mean mole density of dry air (e.g. in mole m^{-3}). The dry CO_2 mixing ratio c (in ppm or μmol mol^{-1}) is measured by a fast-response gas analyser and the vertical wind velocity w (in m s^{-1}) is often measured by a sonic anemometer. The prime denotes the fluctuations from the mean, while the overbar indicates time average. Equation 2 does not rely on ΔfCO_2 measurements nor empirical parameters and assumptions of the gas properties (Wanninkhof, 2014). EC flux measurements can therefore be considered useful as an independent reference for bulk air-sea CO_2 flux estimates. Furthermore, the typical temporal and spatial scales of EC flux measurements are ca. hourly and 1-10 km^2. These scales are much smaller than the temporal and spatial scales of alternative techniques for measuring gas transfer, e.g. by dual tracer methods (daily and 1000 km^2) (Nightingale et al., 2000; Ho et al., 2006). EC

measurements are thus potentially better-suited to capture variations in gas exchange due to small-scale processes at the air-sea interface (Garbe et al., 2014).

The EC CO_2 flux method has developed and improved over time. Before 1990, EC was successfully used to measure air-sea momentum and heat fluxes. EC air-sea CO_2 flux measurements made during those times were unreasonably high (Jones and Smith, 1977; Wesely et al., 1982; Smith and Jones, 1985; Broecker et al., 1986). After 1990, with the development of the infrared gas analyser, EC became routinely used for terrestrial carbon cycle research (Baldocchi et al., 2001). Development of the EC method was accompanied by improvements in the flux uncertainty analysis, which was generally based on momentum, heat and land-atmosphere gas flux measurements (Lenschow and Kristensen, 1985; Businger, 1986; Lenschow et al., 1994; Wienhold et al., 1995; Mahrt, 1998; Finkelstein and Sims, 2001; Loescher et al., 2006; Rannik et al., 2009, 2016; Billesbach, 2011; Mauder et al., 2013; Langford et al., 2015; Post et al., 2015).

In the late 1990s, the advancement in motion correction of wind measurements (Edson et al., 1998; Yelland et al., 1998) facilitated ship-based EC CO_2 flux measurements from a moving platform (McGillis et al., 2001; 2004). After 2000, a commercial open-path infrared gas analyser LI-7500 (Li-COR Inc. USA) became widely used for air-sea CO_2 flux measurements (Weiss et al., 2007; Kondo and Tsukamoto, 2007; Prytherch et al., 2010; Edson et al., 2011; Else et al., 2011; Lauvset et al., 2011). The LI-7500 generated extremely large and highly variable CO_2 fluxes in comparison to expected fluxes (Kondo and Tsukamoto, 2007; Prytherch et al., 2010; Edson et al., 2011; Else et al., 2011; Lauvset et al., 2011). This problem is generally considered to be an artefact caused by water vapour cross-sensitivity (Kohsiek, 2000; Prytherch et al., 2010; Edson et al., 2011; Landwehr et al., 2014). Mathematical corrections proposed to address this artefact (Edson et al., 2011; Prytherch et al., 2010) were later shown to be unsatisfactory (Else et al., 2011; Ikawa et al., 2013; Blomquist et al., 2014; Tsukamoto et al., 2014) or incorrect (Landwehr et al., 2014).

The most reliable method for measuring EC air-sea CO_2 fluxes involves physical removal of water vapour fluctuations from the sampled air. The simplest approach is to combine a closed-path gas analyser with a physical dryer to eliminate most of the water vapour fluctuation (Miller et al., 2010; Blomquist et al., 2014; Landwehr et al., 2014; Yang et al., 2016; Nilsson et al., 2018). The tuneable-diode-laser-based cavity ring-down spectrometer (CRDS) made by

Picarro Inc. (Santa Clara, California, USA) is the most precise closed-path analyser currently available (Blomquist et al., 2014). The closed-path infrared gas analyser LI-7200 (LI-COR Biosciences, Lincoln, Nebraska, USA) is another popular choice.

The advancements in instrumentation and in motion correction methods have significantly improved the quality of air-sea EC CO_2 flux observations but, despite these changes, the flux uncertainties have not been well-quantified. The aims of this study are to: 1) analyse uncertainties in EC air-sea CO_2 flux measurements; 2) propose practical methods to reduce the systematic and random flux uncertainty; and 3) investigate how the EC flux uncertainty influences our ability to estimate and parameterise K_{660}.

2 Experiment and methods

2.1 Instrumental set-up
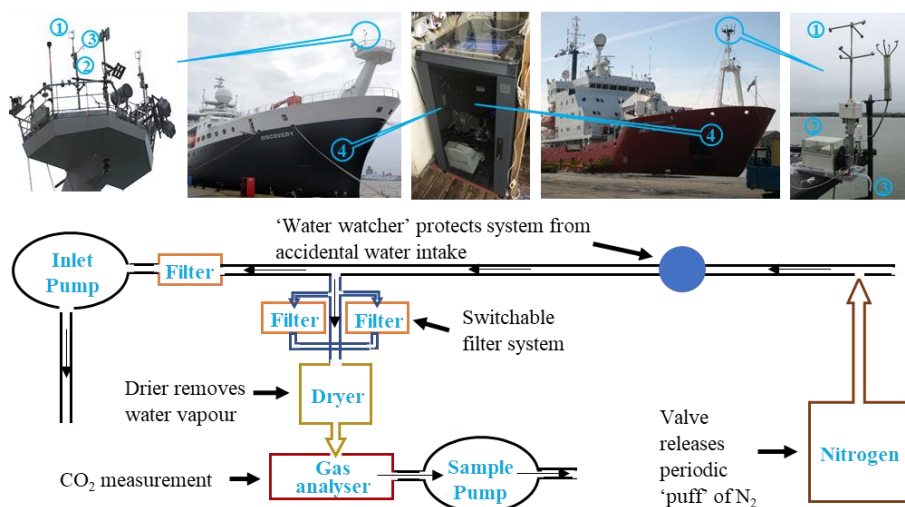
Figure 1. EC system (upper panel) and a diagram of system setup (bottom panel). EC instruments: 1) Sonic anemometer, 2) Motion sensor, 3) Air sample inlet for gas analyser, 4) Datalogger/gas analyser. Arctic and Atlantic data from 2018 were collected on the RRS James Clark Ross (JCR, upper right) using a Picarro G2311-f, and Atlantic data from 2019 were collected using a LI-7200 on the RRS Discovery (upper left).

112

The basic information of four cruises is summarised in Table 1. Appendix A shows the four cruise tracks (Fig. A1, A2). Data from the Atlantic cruises (AMT28 and AMT29) are limited to 3° N–20° S in order to focus specifically on the performance of two different gas analysers in the same region with low flux signal (tropical zone).

117

Table 1. Basic information for all four cruises on the RRS James Clark Ross (JCR) and RRS Discovery that measured air-sea EC CO_2 fluxes.

Cruise	JR18006	JR18007	AMT28	AMT29
Data period	30 June–1 August 2019	5 August–29 September 2019	9 October–16 October 2018	4 November–11 November 2019
Visited region	Arctic Ocean (Barents Sea)	Arctic Ocean (Fram Strait)	Tropical Atlantic Ocean	Tropical Atlantic Ocean
Research vessel	JCR	JCR	JCR	Discovery
Gas analyser	Picarro G2311-f	Picarro G2311-f	Picarro G2311-f	LI-7200

120

The CO_2 flux and data logging systems installed on the JCR and Discovery were operated autonomously. The EC systems were approximately 20 m above mean sea level on both ships (at the top of the foremasts, Fig. 1) to minimise flow distortion and exposure to sea spray. Computational fluid dynamics (CFD) simulation indicates that the airflow distortion at the top of the JCR foremast is small (~1% of the free stream wind speed when the ship is head to wind, Moat and Yelland, 2015). The hull structure of RRS Discovery is nearly identical to that of RRS James Cook. CFD simulation of the James Cook indicates that the airflow at the top foremast is distorted by ~2% for bow-on flows (Moat et al., 2006). The deflection of the streamline from horizontal and effects on the vertical wind component is accounted for by the double rotation (motion correction processes, see Sect. 2.2) prior to the EC flux calculation for both ships.

The EC system on the JCR consists of a three-dimensional sonic anemometer (Metek Inc., Sonic-3 Scientific), a motion sensor (initially Systron Donner Motionpak II, which compared favourably with and was then replaced by a Life Performance-Research LPMS-RS232AL2 in April 2019), and a Picarro G2311-f gas analyser. All instruments sampled at a frequency of 10 Hz or greater and the data were logged at 10 Hz with a datalogger (CR6, Campbell Scientific,

137   Inc.), similar to the setup by Butterworth and Miller (2016). Air is pulled through a long tube

138   (30 m, 0.95 cm inner diameter, Reynolds number 5957) with a dry vane pump at a flow rate of

139   ~40 L min^{-1} (Gast 1023 series). The Picarro gas analyser subsamples from this tube through a

140   particle filter (Swagelok 2 µm) and a dryer (Nafion PD-200T-24M) at a flow of ~5 L min^{-1}

141   (Fig. 1). The dryer is setup in the 're-flux' configuration and uses the lower pressure Picarro

142   exhaust to dry the sample air. This method removes ~80% of the water vapour and essentially

143   all of the humidity fluctuations (Yang et al., 2016). The Picarro internal calculation accounts

144   for the detected residual water vapour and yields a dry CO_2 mixing ratio that is used in the flux

145   calculations. A valve controlled by the Picarro instrument injects a 'puff' of nitrogen (N_2) into

146   the tip of the inlet tube for 30 s every 6 hours. This enables estimates of the time delay and

147   high-frequency signal attenuation (Sect. 2.2).

148   The EC system on RRS Discovery consists of a Gill R3-50 sonic anemometer, a LPMS motion

149   sensor package, and a LI-7200 gas analyser. The LI-7200 gas analyser was mounted within the

150   enclosed staircase, directly underneath the meteorological platform and close to the inlet (inlet

151   length 7.5 m, inner diameter 0.95 cm, Reynolds number 1042). A single pump (Gast 1023) was

152   sufficient to pull air through a particle filter (Swagelok 2 µm), a dryer (Nafion PD-200T-24M),

153   and the LI-7200 at a flow of ~7 L min^{-1}. There was no N_2 puff system setup on Discovery but

154   equivalent lab tests confirmed that the delay time was less than on the JCR because of the

155   shorter inlet line. The dryer on the Discovery is setup in the same 're-flux' configuration as the

156   JCR and uses the lower pressure at the LI-7200 exhaust (limited by an additional 0.08 cm

157   diameter critical orifice) to dry the sample air. This setup removes ~60–70% of the water

158   vapour and essentially all of the humidity fluctuations. The dry CO_2 mixing ratio, computed

159   by accounting for the LI-7200 temperature, pressure and residual water vapour measurements,

160   is used in the flux calculations.

161

162   **2.2 Flux processing**

163   The EC air-sea CO_2 flux calculation steps using the raw data are outlined with a flow chart

164   (Fig. 2) and detailed below. The raw high frequency wind and CO_2 data are processed first,

165   yielding fluxes in 20 min averaging time interval and related statistics. These statistics are then

166   used for quality control of the fluxes. Further averaging of the quality-controlled 20 min fluxes

167   to hourly or longer time scales is then used to reduce random error (Sect. 4.1). Linear

168   detrending was used to identify the turbulent fluctuations (i.e. w' and c') throughout the

169   analyses.

To correct the wind data for ship motion, we first generated hourly data files containing the measurements from the sonic anemometer (three-dimensional wind speed components: u, v and w and sonic temperature Ts), motion sensor (three axis accelerations: accel_x, accel_y, accel_z; and rotation angles: rot_x, rot_y, rot_z), ship heading over ground (HDG, from the gyro compass) and ship speed over ground (SOG, from Global Position System). Spikes larger than 4 standard deviations (SDs) from the median were removed. Secondly, a complementary filtering method using Euler angles (see Edson et al., 1998) was applied to the hourly data files to remove apparent winds generated by the ship movements. The motion-corrected winds were further decorrelated against ship motion to remove any residual motion-sensitivity (Miller et al., 2010; Yang et al., 2013). The motion-corrected winds were double rotated to account for the wind streamline over the ship, yielding the vertical wind velocity (w) required in Eq. 2. Inspection of frequency spectra showed that the spectral peak at the ship motion frequencies (approximately 0.1−0.3 Hz) had disappeared after the motion correction (Fig. S1, Supplement). This indicates that the majority of ship motion had been removed from the measured wind speed. The last step in the wind data processing was the calculation of 20 min average friction velocity, sensible heat flux and other key variables used for data quality control (Table S1, Supplement).

The CO_2 data were de-spiked (by removing values > 4 SDs from the median). The Picarro CO_2 mixing ratio was further decorrelated against analyser cell pressure and temperature to remove CO_2 variations due to ship's motion. The LI-7200 CO_2 mixing ratio was further decorrelated against the LI-7200 H_2O mixing ratio and temperature to remove residual air density fluctuations, following Landwehr et al. (2018). CO_2 data were also decorrelated against ship's heave and accelerations because these can produce spurious CO_2 variability (Miller et al., 2010; Blomquist et al., 2014).

A lag between CO_2 data acquisition and the wind data is created because of the time taken for sample air to travel through the inlet tube. On the JCR, we use the 'puff' system where the lag time is the time difference between the N_2 'puff' start (when the on/off valve is switched) and the time when the diluted signal is sensed by the gas analyser. The lag time can also be estimated by the maximum covariance method, calculated by shifting the time base of the CO_2 signal and finding the shift that achieves maximum covariance between the vertical wind velocity (w) signal and the shifted CO_2 signal. The lag times estimated by the maximum covariance method agree well with the estimates of the 'puff' procedure (Fig. S2, Supplement). These estimates indicate a lag time of 3.3–3.4 s for the Arctic cruises and 3.3 s for cruise

203 AMT28 on the JCR. The maximum covariance method estimated lag time on Discovery
204 (AMT29) was 2.6 s, consistent with laboratory test results prior to the cruise.
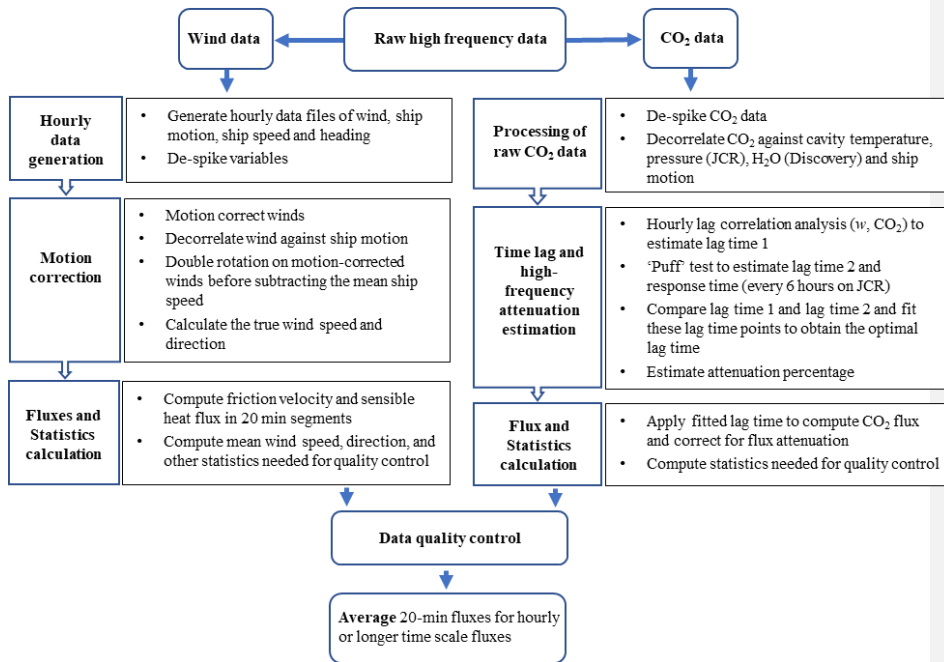
205

206 **Figure 2.** Flow chart of EC data processing. The raw high frequency (10 Hz) wind and CO_2 data were
207 initially processed separately and then combined to calculate fluxes. CO_2 fluxes were filtered by a series
208 of data quality control criteria. The 20-min flux intervals were averaged to longer time scales (hourly
209 or more). The data processing is detailed in the text.

210

211 The inlet tube, particle filter and dryer cause high-frequency CO_2 flux signal attenuation. The
212 N_2 'puff' was also used to assess the response time by considering the e-folding time in the
213 CO_2 signal change (similar approaches have been used by Bariteau et al., 2010; Blomquist et
214 al., 2014, Bell et al., 2015). The response time is 0.35 s for the EC system on JCR and 0.25 s
215 for the EC system on Discovery (estimated in the laboratory prior to cruise). These response
216 times were combined with the relative wind speed-dependent, theoretical shapes of the
217 cospectra (Kaimal et al., 1972) to estimate the percentage flux loss due to the inlet attenuation
218 (Yang et al., 2013). The mean attenuation percentage is less than 10% with a relative wind
219 speed dependence (Fig. S3, Supplement). The attenuation percentage value was applied to the

computed flux to compensate the flux loss due to the high-frequency signal attenuation. Finally, horizontal CO_2 fluxes and other statistics such as CO_2 range and CO_2 trend were computed for quality control purposes (Table S1, Supplement).

The computed 20-min fluxes were filtered for non-ideal ship manoeuvres or violations of the homogeneity/stationary requirement of EC (see Supplement for the quality control criteria).

2.3 Uncertainty analysis methods

2.3.1 Uncertainty components

Uncertainty contains two components: systematic error (δF_S) and random error (δF_R). According to propagation of uncertainty theory (JCGM, 2008), the total uncertainty in EC CO_2 fluxes (from random and systematic errors) can be expressed as:

$$\delta F = \sqrt{\delta F_R{}^2 + \delta F_S{}^2} \tag{3}$$

Systematic errors (Sect. 2.3.2) will cause bias in the flux. They thus should be eliminated/minimised with appropriate system setup and, if needed, effective numerical corrections. Random error results in imprecision (but not bias) and can be reduced by averaging repeated measurements (Sect. 2.3.3). Errors due to insufficient sampling and instrument noise are generally considered most important in EC flux measurements (Lenschow and Kristensen, 1985; Businger 1986; Mauder et al., 2013; Rannik et al., 2016).

Sampling error is an inherent issue for EC flux measurements and is typically the main source of the CO_2 flux uncertainty (Mauder et al., 2013). The sampling error is caused by the difference between the ensemble average and the time average. The calculation of EC flux (Eq. 2) requires the separation between the mean and fluctuating components, which can be represented fully for CO_2 mixing ratio c as:

$$c(x,t) = \bar{c}(x,t) + c'(x,t) \tag{4}$$

The mean component $\bar{c}$ represents ensemble average over time (t) and space (x) and does not contribute to the flux. The time average of a stationary turbulent signal and space average of a homogenous turbulent signal theoretically converge on the ensemble average when the averaging time approaches infinity, i.e. $T \to \infty$ (Wyngaard, 2010). In practice, Reynolds averaging over a much shorter time interval (10 min to an hour) is typically used for EC flux

measurements from a fixed point or from a slow-moving platform such as a ship. This is because the atmospheric boundary layer is only quasi-stationary for a few hours. Non-stationarity (e.g. diurnal variability and synoptic conditions) is an inherent property of the atmospheric boundary layer (Wyngaard, 2010). EC flux obervations thus inevitably contain some random error due to insufficient samping time, and this error is greater at shorter averaging times.

Random error due to instrument noise comes mainly from the white noise of the gas analyser, as the noise from the sonic anemometer is relatively unimportant (Blomquist et al., 2010; Fairall et al., 2000; Mauder et al., 2013). Blomquist et al. (2014) show 'pink' noise with a weak spectral slope for their CRDS gas analyser (G1301-f), but the gas analysers on JCR (G2311-f) and Discovery (LI-7200) demonstrate white noise with a constant variance at high frequency (Fig. B2, Appendix B).

2.3.2 Systematic error

Table 2 details the measures taken during instrument setup and data processing that help eliminate most sources of systematic error in EC CO_2 fluxes.

Table 2. Potential sources of bias in our EC air-sea CO_2 flux measurements and the methods used to minimise them.

Potential source of bias	Methods used to minimise the bias	Flux uncertainty
$\delta F_{S,1}$ **Water vapour cross-sensitivity**	Closed-path gas analyser with a dryer removes essentially all of the water vapour fluctuation (Blomquist et al., 2014; Yang et al., 2016). The residual H_2O signal is measured by the gas analyser and used in the calculation of dry CO_2 mixing ratio, which removes water cross-sensitivity.	Negligible
$\delta F_{S,2}$ **Ship motion**	Flux uncertainty from an earlier version of the motion correction procedure (less rigorous than the one used by ourselves) is estimated to be 10-20% (Edson et al. 1998). The more recently-adopted decorrelation of vertical winds and CO_2 against platform motion (Miller et al., 2010; Yang et al., 2013) reduces this uncertainty. Flügge et al. (2016) compare EC momentum fluxes measured	≤ 6%

	from a moving platform (buoy) with fluxes measured from a nearby fixed tower. Flux estimates from these two platforms agree well (relative flux bias due to the motion correction ≤ 6%).	
$\delta F_{S,3}$ **Airflow distortion**	The EC flux system is deployed as far forward and as high as possible on the ship (top of the foremast), which minimises the impacts of flow distortion. Subsequent distortion correction using the CFD simulation (Moat et al., 2006; Moat and Yelland, 2015) along with a relative wind direction restriction further reduces the impact of flow distortion on the fluxes. Measured EC friction velocities and friction velocities from the COARE3.5 model (Edson et al., 2013) agree well (e.g. $R^2 = 0.95$, slope = 0.97) for data collected during cruise JR18006. Good comparison between observed and COARE3.5 friction velocity estimates indicates that we have fully accounted for flow distortion effects.	Negligible
$\delta F_{S,4}$ **Inlet effects (high-frequency flux attenuation and CO_2 sampling delay)**	High-frequency flux signal attenuation (in the inlet tube, particle filter and dryer) is evaluated by the CO_2 signal response to a puff of N_2 gas. Flux attenuation is calculated from the 'inlet puff' response and applied as a correction (< 10%, see Sect. 2.2). The uncertainty in the attenuation correction is about 1% for unstable/neutral atmospheric conditions, which is generally the case over the ocean (e.g. 93% of the time for the Atlantic cruises, 80% of the time for the Arctic cruises). During stable conditions, the attenuation correction is larger (Landwehr et al., 2018) and the uncertainty is also greater (~20%). The lag time adjustment prior to the flux calculation aligns the CO_2 and wind signals. Two methods are used to estimate the optimal lag time: puff injection and maximum covariance. The two lag estimates are in good agreement (Sect. 2.2). Random adjustment of ± 0.2 s (1 σ of the puff test result) to the optimal lag time impacts the CO_2 flux by < 1%.	< 2% for vast majority of the cruises
$\delta F_{S,5}$ **Spatial separation between the sonic**	The CO_2 inlet is ~70 cm directly below the centre volume of the sonic anemometer. This distance is small relative to the size of the dominant flux-carrying eddies encountered by the EC measurement system height above sea level. The excellent agreement between the lag time determined by the puff system and by the optimal	Negligible

anemometer and the gas inlet	covariance method further confirms that the distance between the CO_2 inlet and anemometer is sufficiently small.	
$\delta F_{S,6}$ **Imperfect calibration of the sensors**	The potential flux bias resulting from instrument calibration (gas analyser, anemometer and meteorological sensors required to calculate air density: air temperature, relative humidity and pressure) is up to 4% for the JCR setup. The largest instrument calibration uncertainty derives from the wind sensor accuracy ($\pm$ 0.15 m s^{-1} at 4 m s^{-1} winds according to the Metek uSonic instrument specification). This bias is even lower (< 2%) for the Discovery setup because the Gill R3 sonic anemometer is more accurate.	$\leq 4\%$
Propagated bias	Estimated from the individual bias estimates above ($\delta F_{S,1}$, $\delta F_{S,2}$, etc.) using $\delta F_S = \sqrt{\sum_1^n \delta F_{S,n}^2}$	$< 7.5\%$

268

269 In addition to bias sources related to the instrument setup (Table 2), insufficient sampling time
270 (an inherent issue of EC fluxes) may also generate a systematic error. We use a theoretical
271 method to estimate this systematic error in EC CO_2 flux (Lenschow et al., 1994):

$$|\delta F_S| \leq 2\sigma_w \sigma_{c_a} \frac{\sqrt{\tau_w \tau_c}}{T} \tag{5}$$

273 where σ_w (m s^{-1}) and σ_{c_a} (ppm) are the standard deviations of the vertical wind velocity and
274 the CO_2 mixing ratio due to atmospheric processes, respectively. T is the averaging time
275 interval (s), and τ_w and τ_c are integral time scales (s) for vertical wind velocity and CO_2 signal,
276 respectively. The definition and estimation of the integral time scale are shown in Appendix B.
277 The sign of δF_S could be positive or negative (i.e. under or over-estimation) because of the
278 poor statistics in capturing low-frequency eddies within the flux averaging period (Lenschow
279 et al., 1993). The mean hourly relative systematic error due to insufficient sampling time for
280 four cruises estimated by Eq. 5 is < 5%. According to propagation of uncertainty theory (JCGM,
281 2008), the total systematic error is less than 9% (= $\sqrt{7.5\%^2 + 5\%^2}$).

2.3.3 Random error

283 Five approaches used to estimate the total random error (A-C) and the random error component
284 due to instrument noise (C-E) in EC CO_2 fluxes are discussed below. The random error
285 assessments are empirical (A and D) or theoretical (B, C and E).

A. An empirical approach to estimate total random error involves shifting the w data relative to the CO_2 data (or vice versa) by a large, unrealistic time shift and then computing the 'null fluxes' from the time-desynchronized CO_2 and w time series (Rannik et al., 2016). The shift removes any real correlation between CO_2 and w due to vertical exchange. The standard deviation of the resultant 'null' fluxes represents the random flux uncertainty (Wienhold et al., 1995). We applied a series of time shifts of $\sim 20 - 60 \times \tau_w$ (i.e. using time shifts ranging from -300 to -100 and 100 to 300 s, Rannik et al., 2016). This empirical estimation of total random flux uncertainty will hereafter be referred to as $\delta F_{R,\text{Wienhold}}$.

B. Lenschow and Kristensen (1985) derived a rigorous theoretical equation for total random error estimation, which contains both the auto-covariance and cross-covariance functions. The theoretical equation has been numerically approximated by Finkelstein and Sims (2001):

$$\delta F_{R,\text{ Finkelstein}} = \left\{ \frac{1}{n} \left[\sum_{p=-m}^{m} r_{ww}(p) r_{cc}(p) + \sum_{p=-m}^{m} r_{wc}(p) r_{cw}(p) \right] \right\}^{1/2} \tag{6}$$

where n is the number of data points within an averaging time interval, p is the number of shifting points. The maximum shifting point m can be chosen subjectively ($< n$). We found that the random error for m between 1000 and 2000 data points was similar, so for this study we use $m = 1500$ (150 s shift time). The first term in the brackets represents the auto-covariance component and the second term is the cross-covariance component. r_{ww} and r_{cc} are the auto-covariance functions for vertical wind velocity (w) and CO_2 mixing ratio (c), respectively. r_{wc} and r_{cw} are the cross-covariance functions for w and c. Here r_{wc} represents shifting w data relative to CO_2 data, while r_{cw} represents shifting CO_2 data relative to w data.

C. Blomquist et al. (2010) attributed the sources of CO_2 variance σ_c^2 to atmospheric processes ($\sigma_{c_a}^2$) and white noise ($\sigma_{c_n}^2$). The sources of variance are considered to be independent of each other and the sonic anemometer is assumed to be relatively noise-free. According to propagation of uncertainty theory (JCGM, 2008), the total random flux error can be defined as:

$$\delta F_{R,\text{ Blomquist}} \leq \frac{a\sigma_w}{\sqrt{T}} \left(\sigma_{c_a}^2 \tau_{wc} + \sigma_{c_n}^2 \tau_{c_n} \right)^{1/2} \tag{7}$$

where the constant a varies from $\sqrt{2}$ to 2, depending on the relationship between the covariance of the two variables (w and CO_2) and the product of their auto-correlations (Lenschow and Kristensen, 1985). Here, τ_{wc} is equal to the shorter of τ_w and τ_c, which is typically τ_w (Blomquist et al., 2010), and τ_{c_n} is the integral time scale of white noise in the CO_2 signal. The CO_2 variance due to atmospheric processes ($\sigma_{c_a}^2$) includes two components: variance due to

vertical flux (i.e. air-sea CO_2 flux) $\sigma^2_{c_{av}}$, and variance due to other atmospheric processes $\sigma^2_{c_{ao}}$ (Fairall et al., 2000). The variance in CO_2 due to vertical flux ($\sigma^2_{c_{av}}$) depends on atmospheric stability. $\sigma^2_{c_{av}}$ can be estimated with Monin-Obukhov similarity theory (Blomquist et al., 2010, 2014; Fairall et al., 2000):

$$\sigma^2_{c_{av}} = \left[3\frac{\overline{w'c'}}{u_*}f_c(z/L)\right]^2 \tag{8}$$

where u_* is the friction velocity (m s^{-1}) and the similarity function (f_c) depends on the stability parameter z/L, where z is the observational height (m) and L is the Obukhov length (m). The expression of f_c can be found in Blomquist et al. (2010).

Equation 7 can be used to assess the random error due to instrument noise by setting $\sigma^2_{c_a} = 0$, referred to hereafter as $\delta F_{RN,\,Blomquist}$. We use the CO_2 variance spectra to directly estimate the white noise term $\sigma^2_{c_n}\tau_{c_n}$ in Eq. 7. The variance is fairly constant at high frequency (1-5 Hz; Fig. B2, Appendix B), which is often referred to as band-limited white noise. The relationship between $\sigma^2_{c_n}\tau_{c_n}$ and the band-limited noise spectral value φ_{c_n}, is expressed in Blomquist et al. (2010) as:

$$\sigma^2_{c_n}\tau_{c_n} = \frac{\varphi_{c_n}}{4} \tag{9}$$

D. Billesbach (2011) developed an empirical method to estimate the random error due to instrument noise alone (referred to as $\Delta F_{RN,\,Billesbach}$). This involves random shuffling of the CO_2 time series within an averaging interval and then calculating the covariance of w and CO_2. The correlation between w and CO_2 is minimized by the shuffling, and any remaining correlation between w and CO_2 is due to the unintentional correlations contributed by instrument noise.

E. Mauder et al. (2013) describe another theoretical approach to estimate the random flux error due to instrument noise:

$$\delta F_{RN,\,Mauder} = \frac{\sigma_w \sigma_{c_n}}{\sqrt{n}} \tag{10}$$

White noise correlates with itself but is uncorrelated with atmospheric turbulence. Thus, the white noise-induced CO_2 variance (σ_{c_n}) only contributes to the total variance. The value of σ_{c_n} can be estimated from the difference between the zero-shift auto-covariance value (CO_2

variance σ_c^2) and the noise-free variance extrapolated to a time shift of zero (Lenschow et al., 2000):

$$\sigma_{c_n}^2 = \sigma_c^2 - \sigma^2(t \to 0) \tag{11}$$

where $\sigma^2(t \to 0)$ represents the extrapolation of auto-covariance to a zero shift, which is considered equal to variance due to atmospheric processes ($\sigma_{c_a}^2$). Figure 3 shows the normalised auto-covariance function curves of w and CO_2 as measured by the Picarro G2311-f and the LI-7200. There is a sharp decrease in the CO_2 auto-covariance when shifting from 0 s shift to 0.1 s shift for both the Picarro G2311-f and LI-7200 gas analyser. The same sharp decrease is not seen in the vertical wind velocity (w) auto-covariance. The relative difference in the change in normalised auto-covariance shows that white noise makes a much larger relative contribution to the CO_2 variance than to the vertical wind velocity variance.
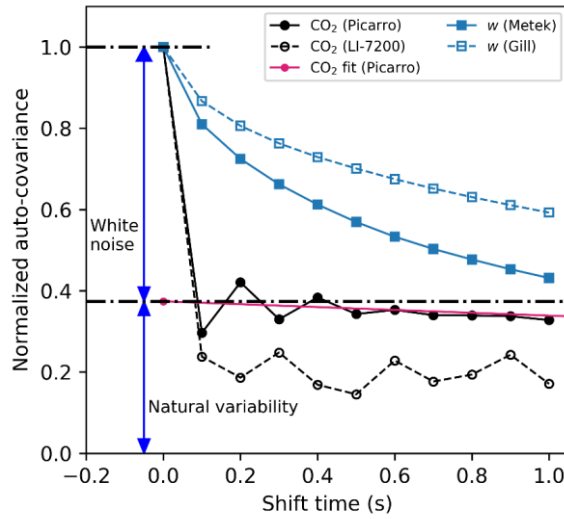
Figure 3. Mean normalised auto-covariance functions of CO_2 and vertical wind velocity (w) by four different instruments. The magenta line represents a fit to the noise-free auto-covariance function of CO_2 (measured by Picarro) extrapolated back to a zero time shift. An example of the white noise and natural variability contributions to the total CO_2 (measured by Picarro) variance is indicated by two blue arrows. The sharp decrease of the CO_2 auto-covariance between the zero shift and the initial 0.1 s shift corresponds to the large contribution of white noise from the gas analysers. The LI-7200 is the noisier instrument. The noise contributions from the anemometer are relatively small ($< 10\%$).

3 Results

Measurements from AMT28 and AMT29 set the scene for our uncertainty analysis. These two Atlantic cruises transited across the same tropical region (Fig. A2, Appendix A) in October 2018 and September 2019 with different eddy covariance systems (Sect. 2.1). AMT28 and AMT29 show broadly similar latitudinal patterns (Fig. 4a). An obvious question of interest is whether the measured fluxes were the same for the two years. To answer this question, the measurement uncertainties must be quantified. The total random uncertainties in CO_2 flux ($\delta F_{R,\,\text{Finkelstein}}$) are comparable for the two cruises even though the random error component due to instrument noise ($\delta F_{RN,\,\text{Mauder}}$) is about 3 times higher during AMT29 using LI-7200 than during AMT28 using Picarro G2311-f (Fig. 4b; Fig. D1, Appendix D). The similar total random uncertainty in the AMT28 and AMT29 fluxes shows that both gas analysers are equally suitable for air-sea EC CO_2 flux measurements. The variance budgets of atmospheric CO_2 mixing ratio (used to estimate random flux uncertainty, see Sect. 3.1) are shown in Fig. 4c. Total variance in CO_2 mixing ratio is dominated by instrument noise on both cruises. CO_2 mixing ratio variance (total and instrument noise) was substantially higher during AMT29.
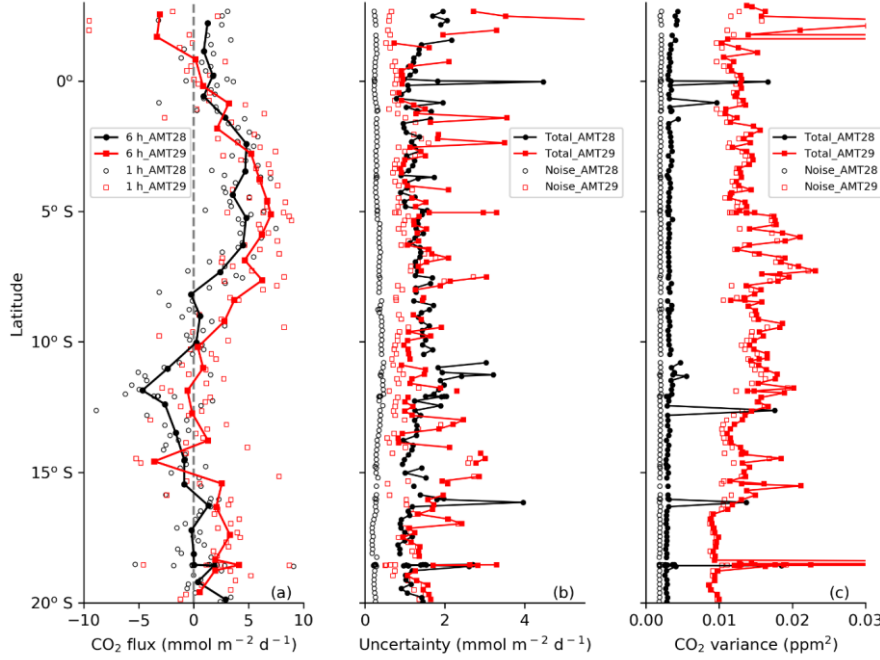
Figure 4. (a) Air-sea CO_2 fluxes (hourly and 6-h averages), (b) random uncertainty in flux (total and due to instrument noise only), and (c) variance in CO_2 mixing ratio (total and due to instrument noise only) for two Atlantic cruises.

3.1 Random uncertainty

Theoretical derivation of flux uncertainty ($\delta F_{RN,\,\text{Blomquist}}$, Eq. 7) requires knowledge of the contributions to CO_2 mixing ratio variance. Total CO_2 variance is made up of instrument noise ($\sigma_{c_n}^2$) and atmospheric processes ($\sigma_{c_a}^2$). Atmospheric processes include vertical flux ($\sigma_{c_{av}}^2$) and other atmospheric processes ($\sigma_{c_{ao}}^2$). The variance budgets of CO_2 mixing ratio for the four cruises are listed in Table 3. Atmospheric processes contribute a larger CO_2 variance in the Arctic (where flux magnitudes are greater) compared to the Atlantic. Vertical flux accounts for ~10% of the variance in CO_2 mixing ratio in the Arctic and ~1% of the CO_2 variance in the Atlantic. Previous results demonstrate that horizontal transport is a major source of $\sigma_{c_{ao}}^2$ for long-lived greenhouse gases (Blomquist et al., 2012). Small changes in CO_2 mixing ratio transported horizontally can yield variance that greatly exceeds the variance from vertical flux.

Table 3. Variance in the CO_2 mixing ratio estimated using Eq. 8 and 11 for the Arctic (JR18006/7, Picarro G2311-f) and Atlantic cruises (AMT28, Picarro G2311-f; AMT29, LI-7200). Total CO_2 variance (σ_c^2) consists of white noise ($\sigma_{c_n}^2$) and atmospheric processes ($\sigma_{c_a}^2$). The latter can be further broken down to the CO_2 variance due to vertical flux ($\sigma_{c_{av}}^2$) and due to other processes ($\sigma_{c_{ao}}^2$).

CO_2 variance ($\times 10^{-3}$ ppm^2)	JR18006	JR18007	AMT28	AMT29
Total, σ_c^2	9.9	8.6	3.6	13.9
Due to instrument white noise, $\sigma_{c_n}^2$	5.8	5.4	2.0	12.6
Due to atmospheric processes, $\sigma_{c_a}^2$	4.1	3.3	1.6	1.3
- Due to vertical flux, $\sigma_{c_{av}}^2$	1.3	0.8	0.03	0.08
- Due to other atmospheric processes, $\sigma_{c_{ao}}^2$	2.8	2.5	1.6	1.2

399

Three quasi-independent methods were used to estimate random uncertainty in EC air-sea CO_2 fluxes caused by instrument noise (δF_{RN}, Methods C-E, Sect. 2.3.3). Good agreement was found between all three estimates (Fig. C2, Appendix C) when $\sqrt{2}$ is used as the constant in Eq. 7 (*a*). The $\Delta F_{RN, \text{Billesbach}}$ estimates have more scatter and are slightly higher than the theoretical results, possibly because the random shuffling of data fails to fully exclude the contribution from atmospheric turbulence (Rannik et al., 2016). For the remainder of this study, we use the $\delta F_{RN, \text{Mauder}}$ method to estimate δF_{RN}.

We used three methods to estimate the total random uncertainty (δF_R, Methods A-C, Sect. 2.3.3) in the hourly-averaged air-sea CO_2 fluxes. There is good agreement among the three estimates (r > 0.88; Fig. C1, Appendix C). Again, the constant in Eq. 7 (*a*) is set to $\sqrt{2}$, as informed by the instrument noise uncertainty analysis above. We use $\delta F_{R, \text{Finkelstein}}$ (Eq. 6) to estimate the total random flux uncertainty hereafter. Our decision is based on $\delta F_{R, \text{Finkelstein}}$ not requiring the integral time scale (unlike $\delta F_{R, \text{Blomquist}}$) and showing less scatter than $\delta F_{R, \text{Wienhold}}$.

Figure 5 shows the different relative contributions to the random flux uncertainty for the Arctic cruises (hourly average). Here the uncertainty is normalised by the flux magnitude and then averaged into flux magnitude bins. When the flux magnitude is sufficiently large (> 20 mmol m^{-2} day^{-1}), the total relative random uncertainty in flux asymptotes to about 15% and is driven by variance associated with both vertical flux and other atmospheric processes. This estimate is similar to uncertainties in air-sea fluxes of other well resolved (i.e. high signal-to-noise ratio) variables (Fairall et al., 2000). At a lower flux magnitude, uncertainty due to atmospheric

420 processes other than vertical flux dominates the total random uncertainty. Uncertainty due to
421 the white noise from the Picarro G2311-f gas analyser is small.

422
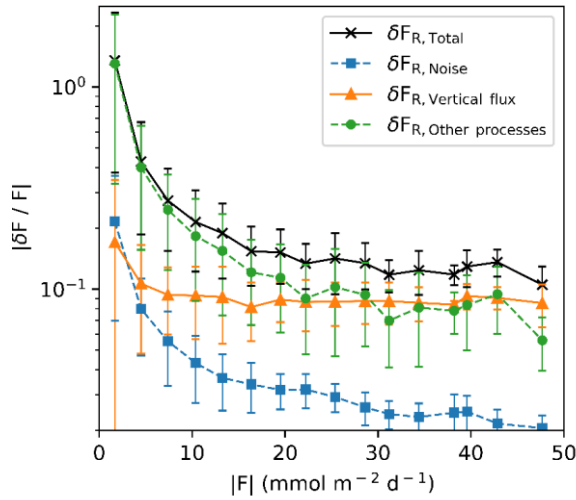
Figure 5. Relative random uncertainty in hourly CO_2 flux and its contribution from noise, vertical flux
and other processes during two Arctic cruises. Relative random uncertainty data are binned into 3 mmol
m^{-2} day^{-1} flux magnitude bins (error bars represent 1 standard deviation).

426

3.2 Summary of systematic and random uncertainties

428 The total uncertainty δF in the hourly average EC CO_2 flux (estimated using Eq. 3) ranges
429 from 1.4 to 3.2 mmol m^{-2} day^{-1} in the mean for the four cruises (Table 4). Our EC flux system
430 setup was optimal and subsequent corrections have minimised any bias to < 9% (Sect. 2.3.2).
431 Systematic error is on average much lower than random error (Table 4). This means the
432 accuracy of the EC CO_2 flux measurements is very high, but the precision of hourly averaged
433 EC CO_2 air-sea flux measurements is relatively low. In Sect. 4.1, we discuss how the precision
434 can be improved by averaging the observed fluxes for longer.

435

436 **Table 4.** Summary of hourly average EC CO_2 fluxes and associated uncertainties in the mean for the
437 four cruises (mmol m^{-2} day^{-1}). Shown are the mean CO_2 flux magnitude ($\overline{|F|}$, mmol m^{-2} day^{-1}), upper
438 limitation of the total uncertainty (δF, Eq. 3), upper limitation of the absolute systematic error ($|\delta F_S|$,

propagated from Table 2 and Eq. 5), and random error (δF_R, Eq. 6). The random error components are white noise (δF_{RN}, Eq. 10), vertical flux (δF_{RV}, Eq. 7 and 8) and other atmospheric processes ($\delta F_{RO} = \sqrt{\delta F_R^2 - \delta F_{RN}^2 - \delta F_{RV}^2}$). The total uncertainty is also expressed as a % of the mean flux magnitude ($\delta F / |F| \times 100\%$).

Cruises	JR18006	JR18007	AMT28	AMT29
$|CO2\ flux|, \overline{|F|}$	10.1	16.3	2.5	3.5
Total uncertainty, δF	2.3	3.2	1.4	1.7
($\delta F / |F| \times 100\%$)	(23%)	(20%)	(58%)	(49%)
Systematic error, $|\delta F_S|$	0.8	1.2	0.3	0.3
Total random error, δF_R	2.2	2.9	1.4	1.7
Random error due to white noise, δF_{RN}	0.5	0.6	0.3	1.0
Random error due to vertical flux, δF_{RV}	1.1	1.4	0.2	0.4
Random error due to other atmospheric processes, δF_{RO}	1.5	2.4	1.4	1.5

The theoretical uncertainty estimates above can be compared with a portion of the AMT28 cruise data (15°–20° S, ~25° W; Fig. 4), when the ship encountered sea surface CO_2 fugacity close to equilibrium with the atmosphere (i.e. $\Delta f CO_2 \sim 0$, Fig. A2, Appendix A). The data from this region is useful for assessing the random and systematic flux uncertainties. The standard deviation of the EC CO_2 flux during cruise AMT28 when $\Delta f CO_2 \sim 0$ is 1.6 mmol m^{-2} day^{-1}, which compares well with the theoretical random flux uncertainty in this region (1.4 mmol m^{-2} day^{-1}). The mean EC CO_2 flux from this region was 0.5 mmol m^{-2} day^{-1}, which is indistinguishable from zero considering the random uncertainty. This further confirms the minimal bias in our flux observations.

Figure 6 shows a comparison between the relative uncertainty and the relative standard deviation (RSTD) in in the hourly CO_2 flux for the two Arctic cruises. Results have been binned into 1 m s^{-1} wind speed bins. Wind speed was converted to 10-meter neutral wind speed (U_{10N}) using the COARE3.5 model (Edson et al., 2013). The relative random error decreases with increasing wind speed. This is partly because the fluxes tend to be larger at higher wind speeds and so the signal-to-noise ratio in the flux is greater. In addition, at higher wind speeds, a greater number of high-frequency turbulent eddies are sampled by the EC system, providing better statistics of turbulent eddies, and lower sampling error.
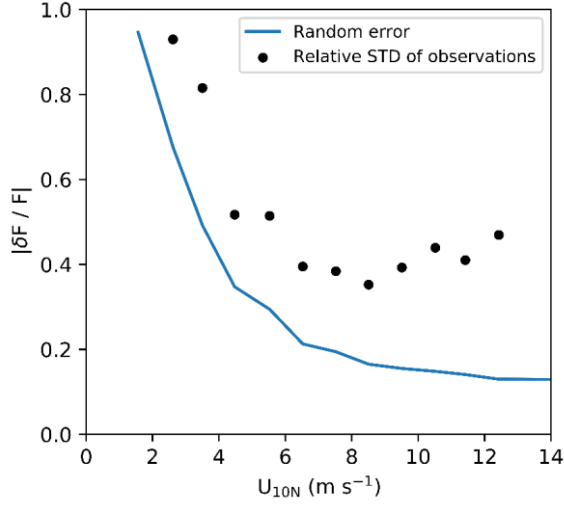
Figure 6. Comparison of relative random uncertainty in hourly CO_2 flux and relative standard deviation (RSTD, standard deviation/|flux mean|) of the EC CO_2 flux from two Arctic cruises. These results are binned in 1 m s^{-1} wind speed bins.

The RSTD of the flux is greater in magnitude than the estimated flux uncertainty because it also contains environmental variability. The CO_2 flux auto-covariance analysis (Sect. 4.1) shows that random error in hourly flux explains ~20% of the flux variance on average for the two Arctic cruises. This implies that the remaining variability in the EC flux (~80%) is due to natural phenomena (e.g. changes in $\Delta f CO_2$, wind speed, etc). Similarly, substantial variability is typical in EC-derived CO_2 gas transfer velocity at a given wind speed (e.g. Edson et al., 2011; Butterworth and Miller, 2016). K_{660} is derived from (EC CO_2 flux)$/\Delta f CO_2$, and thus an understanding of EC flux uncertainty can help understand and explain the variability in EC-derived gas transfer velocity estimates (Sect. 4.2).

4 Discussion

4.1 Impact of averaging time scale on flux uncertainty

The random error in flux decreases with increasing averaging time interval T or the number of sampling points n (Eq. 6, 7 and 10). This is because a longer averaging time interval results in better statistics of the turbulent eddies. However, averaging for too long is also not ideal since

480 the atmosphere is less likely to maintain stationarity. The typical averaging time interval is thus
481 typically between 10 min and 60 min for air-sea flux measurements (20 min intervals were
482 used in this study). The timeseries of quality controlled 20 min flux intervals can be further
483 averaged over a longer time scale to reduce the random uncertainty. Averaging the 20 min flux
484 intervals assumes that the flux interval data are essentially repeat measurements within a
485 chosen averaging time scale. If the 20 min flux intervals are averaged, one can ask: What is the
486 optimal averaging time scale for interpreting air-sea EC CO_2 fluxes?

487 We use an auto-covariance method to determine the optimal averaging time scale. The observed
488 variance in CO_2 flux consists of random uncertainty (random noise) as well as natural
489 variability. The random noise component should only contribute to the CO_2 flux variance when
490 the data are zero-shifted. After the CO_2 flux data are shifted, the noise will not contribute to the
491 auto-covariance function. Figure 7 shows the auto-covariance function of the air-sea CO_2 flux
492 with different averaging time scales for Arctic cruise JR18007. For the 20-min fluxes (Fig. 7a),
493 the auto-covariance decreases rapidly between the zero shift and the initial time shift, which
494 indicates that a large fraction of the 20-min flux variance is due to random noise.

495
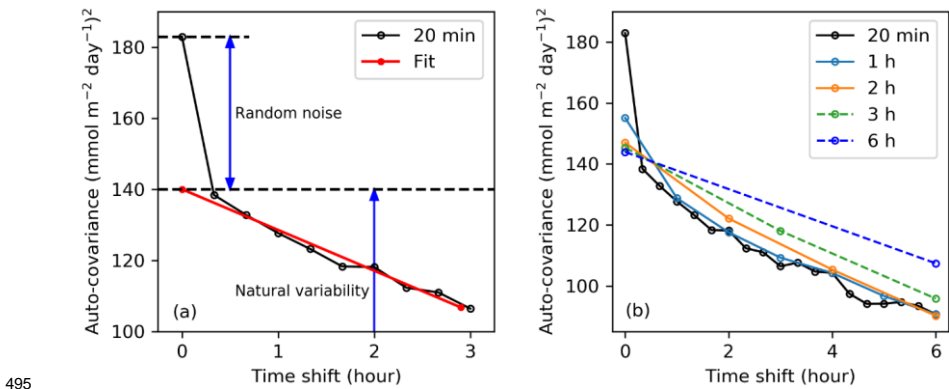
496 **Figure 7.** (a) Auto-covariance of the original 20-min fluxes (cruise JR18007) and a fit to the noise-free
497 auto-covariance function extrapolated back to a zero time shift. (b) CO_2 flux auto-covariance functions
498 with different averaging time scales. The black line represents the auto-covariance of the original 20-
499 min fluxes. The 20-min fluxes are further averaged at different time scales (1, 2, 3 and 6 hour) and the
500 corresponding auto-covariance functions are shown with different colours (dark blue, orange, green and
501 light blue).

502

The random noise in the CO_2 fluxes decreases with a longer averaging time scale, with the greatest effect observed from 20 min to 1 hour (Fig. 7b). A fit to the noise-free auto-covariance function extrapolated back to a zero time shift gives us an estimate of the non-noise variability in the natural CO_2 flux. Subtracting the extrapolated natural flux variability from the total variance in CO_2 flux provides an estimate of the random noise in the flux for each averaging timescale (Fig. 7a). All four cruises consistently demonstrate a non-linear reduction in the noise contribution to the flux measurements when the averaging timescale increases (Fig. 8). The random noise in flux can be expressed relative to the natural variance in flux representing the inverse of the signal-to-noise ratio (i.e. random noise in flux/natural flux variability , hereafter referred to as noise:signal).
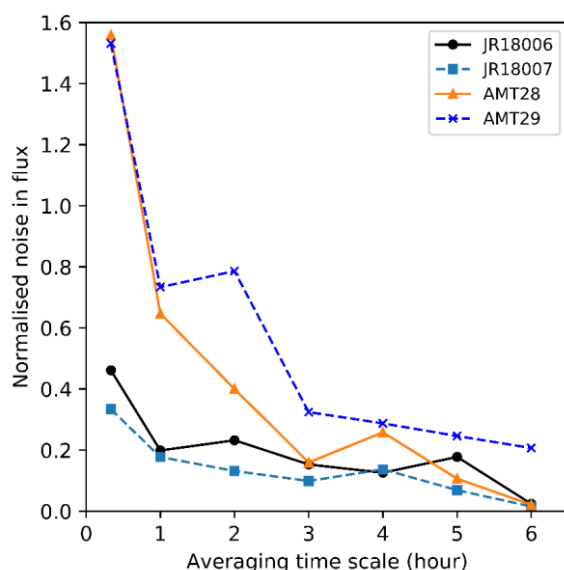
Figure 8. Effect of the averaging timescale on the noise: signal (random noise in flux/ natural flux variability) for EC air-sea CO_2 flux measurements during four cruises.

The noise:signal also facilitates comparison of all four cruises (Fig. 8) and demonstrates the consistent effect that increasing the averaging timescale has on noise:signal. Consistent with Table 4, the Arctic cruises show much lower noise:signal because the flux magnitudes are much larger. Typical detection limits in analytical science are often defined by a 1:3 noise: signal ratio. A 1:3 noise:signal is achieved with a 1 h averaging timescale for the Arctic cruises.

522 The Atlantic cruises encountered much lower air-sea CO_2 fluxes and an averaging timescale of

523 at least 3 h is required to achieve the same 1:3 noise:signal ratio.

524 The flux measurement uncertainty at a 6-h averaging timescale for the AMT cruises is ~0.6

525 mmol m^{-2} day^{-1}. The analysis presented above permits an answer to the question posed at the

526 beginning of the Results section. The mean difference between the 6-h averaged EC CO_2 flux

527 observations on AMT29 and AMT28 (1.3 mmol m^{-2} day^{-1}, Fig. 4a) is much greater than the

528 measurement uncertainty. This significant difference was likely because of the interannual

529 variability in AMT CO_2 flux due to changes in the natural environment (e.g. $\Delta f CO_2$, sea surface

530 temperature, and physical drivers of interfacial turbulence such as wind speed) during the two

531 cruises.

532 At a typical research ship speed of ~10 knots, the AMT cruises cover ~110 km in 6 h, which is

533 equivalent to ~1° latitude. Averaging for longer than 6 h is likely to cause substantial loss of

534 real information about the natural variations in air-sea CO_2 flux and the drivers of flux

535 variability. For example, the mean flux between 0–20° S during cruise AMT28 is 0.9 mmol m^{-}

536 ^{2} day^{-1}. However, the 6 h average EC measurements show that the flux varied between +5 mmol

537 m^{-2} day^{-1} (~2–6° S) and -5 mmol m^{-2} day^{-1} (~11–13° S, Fig. 4a).

538

4.2 Effect of CO_2 flux uncertainty on the gas transfer velocity K

540 The uncertainties in the EC CO_2 air-sea flux measurement will influence the uncertainty that

541 translates to EC-based estimates of the gas transfer velocity, K. For illustration, K is computed

542 for Arctic cruise JR18007, which had a high flux signal:noise ratio of ~5 (Fig. 8). Any data

543 potentially influenced by ice and sea ice melt were excluded using a sea surface salinity filter

544 (data excluded when salinity < 32). Equation 1 is rearranged and used with concurrent

545 measurements of CO_2 flux (F), $\Delta f CO_2$, and sea surface temperature (SST) to obtain K adjusted

546 for the effect of temperature (K_{660}).

547 The determination coefficient (R^2) of the quadratic fit between wind speed (U_{10N}) and EC-

548 derived K_{660} (Fig. 9) demonstrates that wind speed explains 76% of the K_{660} variance during

549 Arctic cruise JR18007. How much of the remaining 24% can be attributed to uncertainties in

550 EC CO_2 fluxes?

551

552
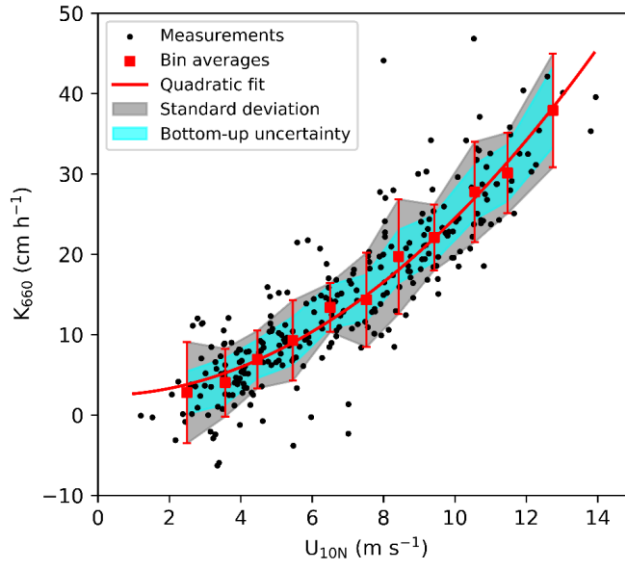
Figure 9. Gas transfer velocity (K_{660}) measured on Arctic cruise JR18007 (hourly average, signal:noise
~5) versus 10-m neutral wind speed (U_{10N}). Red squares represent 1 m s^{-1} bin averages with error bars
representing one standard deviation (SD). The red curve represents a quadratic fit using the bin averages:
$K_{660} = 0.22U_{10N}^2 + 2.46$ (R^2 = 0.76). The grey shaded area represents the standard deviation calculated
for each wind speed bin ($K_{660} \pm 1SD$). The cyan region represents the upper and lower bounds in K_{660}
uncertainty computed from the EC flux uncertainty ($K_{660} \pm \delta K_{660}$, see text for detail).

559

Variability in K_{660} within each 1 m s^{-1} wind speed bin can be considered to have minimal wind
speed influence. It is thus useful to compare the variability within each wind speed bin ($K_{660} \pm$
1SD) with the upper and lower uncertainty bounds derived from the EC flux measurements.
Uncertainty in EC flux-derived K_{660} (δK_{660}) is calculated from the uncertainty in hourly EC
flux (δF) by rearranging Eq. 1 (bulk flux equation) and replacing F with δF. The resultant δK_{660}
is then averaged in wind speed bins. The shaded cyan band in Fig. 9 ($K_{660} \pm \delta K_{660}$) is
consistently narrower than the grey shaded band ($K_{660} \pm 1SD$). On average, EC flux-derived
uncertainty in K_{660} can only account for a quarter of the K_{660} variance within each wind speed
bin and the remaining variance is most likely due to the non-wind speed factors that influence
gas exchange (e.g. breaking waves, surfactants).

The analysis above can be extended to assess how EC flux-derived uncertainty affects our ability to parameterise K_{660} (e.g. as function of wind speed). To do so, a set of synthetic K_{660} data is generated (same U_{10N} as the K_{660} measurements in Fig. 9). The synthetic K_{660} data are initialised using a quadratic wind speed dependence that matches JR18007 (i.e. $K_{660} = 0.22U_{10N}^2 + 2.46$). Random Gaussian noise is then added to the synthetic K_{660} data, with relative noise level corresponding to the relative flux uncertainty values taken from JR18007 (mean of 20%, Table 4). The relative uncertainty in K_{660} due to EC flux uncertainty ($\delta K_{660}/K_{660}$) shows a wind speed dependence (Fig. S4a, Supplement), and the artificially-generated Gaussian noise incorporates this wind speed dependence (Fig. S4b, Supplement). The R^2 of the quadratic fit to the synthetic data as a function of U_{10N} is 0.90 (the rest of the variance is due to uncertainty in K_{660}). Since wind speed explains 76% of variance in the observed K_{660}, it can be inferred that non-wind speed factors can account for 14% (i.e. (100-76)% - (100-90)%) of the total variance in K_{660} from this Arctic cruise. If the synthetic K_{660} data is assigned a relative flux uncertainty of 50% (reflective of a region with low fluxes, e.g. AMT28/29), the R^2 of the wind speed dependence in the synthetic data decreases to 0.60.

The relative uncertainty in EC flux-derived K_{660} ($\delta K_{660}/K_{660}$) is large when $|\Delta fCO_2|$ is small (Fig. 10). Previous EC studies have filtered EC flux data to remove fluxes when the $|\Delta fCO_2|$ falls below a specified threshold (e.g. 20 µatm, Blomquist et al. (2017); 40 µatm, Miller et al. (2010), Landwehr et al. (2014), Butterworth and Miller (2016), Prytherch et al. (2017); 50 µatm, Landwehr et al. (2018)). Analysis of the data presented here suggests that a $|\Delta fCO_2|$ threshold of at least 20 µatm is reasonable for hourly K_{660} measurements, leading to δK_{660} of ~10 cm h^{-1} ($\delta K_{660}/K_{660}$ ~1/3) or less on average. At very large $|\Delta fCO_2|$ of over 100 µatm, δK_{660} is reduced to only a few cm h^{-1} ($\delta K_{660}/K_{660}$ ~1/5). At longer flux averaging time scales, it may be possible to relax the minimal $|\Delta fCO_2|$ threshold.
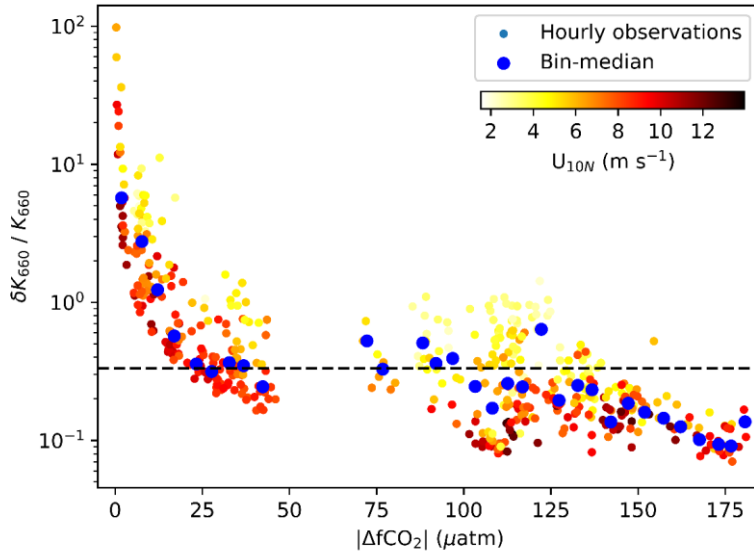
Figure 10. Relative uncertainty in EC-estimated hourly K_{660} ($\delta K_{660}/K_{660}$) versus the magnitude of the air-sea CO_2 fugacity difference ($|\Delta fCO_2|$) during Arctic cruise JR18007 and Atlantic cruises AMT28 and AMT29 (no ΔfCO_2 data were collected on JR18006). The data points are colour-coded by wind speed. Blue points are medians of $\delta K_{660}/K_{660}$ in 5 µatm bins. Here we use the parameterised K_{660} (= $0.22U_{10N}^2 + 2.46$) to normalise the uncertainty in K_{660}. The dashed line represents the 3:1 signal:noise ratio ($\delta K_{660}/K_{660} = 1/3$).

5. Conclusions

This study uses data from four cruises with a range in air-sea CO_2 flux magnitude to comprehensively assess the sources of uncertainty in EC air-sea CO_2 flux measurements. Data from two ships and two different state-of-the-art CO_2 analysers (Picarro G2311-f and LI-7200, both fitted with a dryer) are analysed using multiple methods (Sect. 2.3). Random error accounts for the majority of the flux uncertainty, while the systematic error (bias) is small (Table 4). Random flux uncertainty is primarily caused by variance in CO_2 mixing ratio due to atmospheric processes. The random error due to instrument noise for the Picarro G2311-f is threefold smaller than for LI-7200 (Table 4 and Fig. D1, Appendix D). However, the contribution of the instrument noise to the total random uncertainty is much smaller than the

612 contribution of atmospheric processes such that both gas analysers are well suited for air-sea
613 CO_2 flux measurements.

614 The mean uncertainty in hourly EC flux is estimated to be 1.4–3.2 mmol m^{-2} day^{-1}, which
615 equates to the relative uncertainty of ~20% in high CO_2 flux regions and ~50% in low CO_2 flux
616 regions. Lengthening the averaging timescale can improve the signal:noise ratio in EC CO_2
617 flux through the reduction of random uncertainty. Auto-covariance analysis of CO_2 flux is used
618 to quantify the optimal averaging timescale (Fig. 7 and 8, Sect. 4.1). The optimal averaging
619 timescale varies between 1 hour for regions of large CO_2 flux (Arctic in our analysis) and at
620 least 3 hours for regions of low CO_2 flux (tropical/sub-tropical Atlantic in our analysis).

621 The measurement uncertainty in EC CO_2 flux contributes directly to scatter in the derived gas
622 transfer velocity, K_{660}. Flux uncertainties determined in this paper are applied to a synthetic
623 K_{660} dataset. This enables a partitioning of the variance in measured K_{660} that is due to EC CO_2
624 flux uncertainty, wind speed, and other processes (10%, 76%, 14% for Arctic cruise JR18007).
625 At a given averaging timescale, a $|\Delta fCO_2|$ threshold helps to reduce the scatter in K_{660}. A
626 minimum $|\Delta fCO_2|$ filter of 20 μatm is needed for interpreting hourly K_{660} data, with the signal:
627 noise ratio in K_{660} improving further at higher $|\Delta fCO_2|$.

628

629

630 **Appendix A: Cruise tracks**
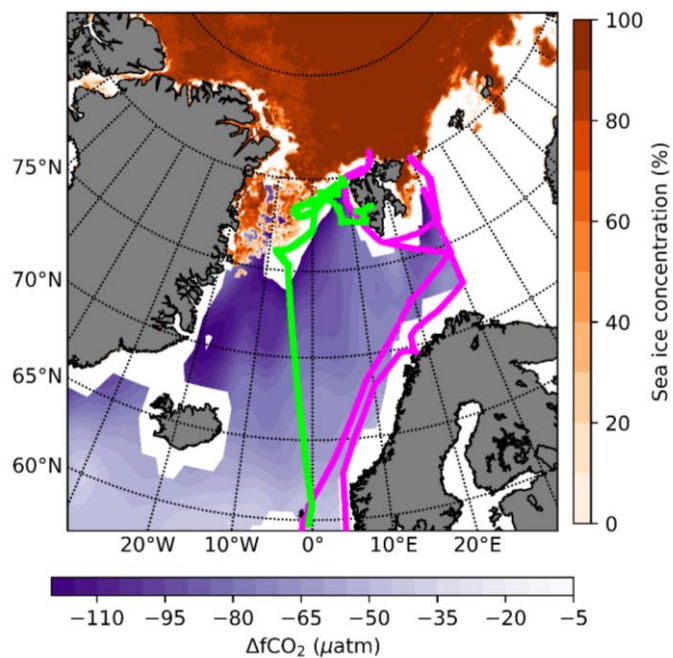
Figure A1. Cruise tracks of JR18006 (magenta) and JR18007 (green). The bottom colour bar indicates the CO_2 fugacity difference ($\Delta f CO_2$) of August 2019 (Bakker et al., 2016; Landschützer et al., 2020), while the right colour bar shows the Arctic sea ice concentrations of 1st August 2019 measured by Advanced Microwave Scanning Radiometer - Earth Observing System Sensor (AMSR-E, Spreen et al., 2008).
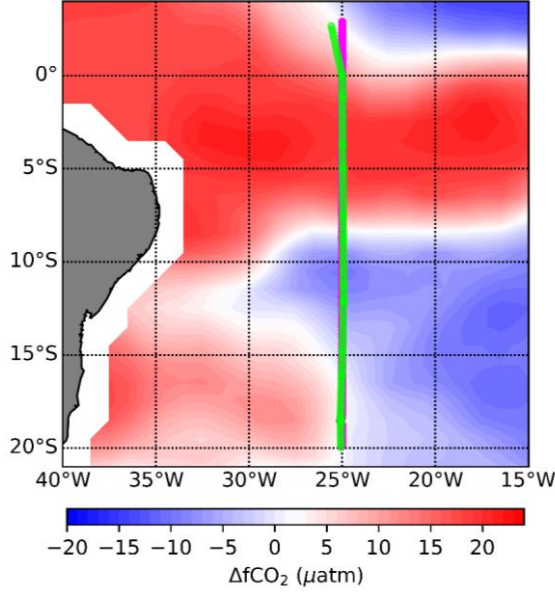
Figure A2. Cruise tracks of AMT28 (magenta) and AMT29 (green). The ocean is coloured with the $\Delta f\mathrm{CO_2}$ for October 2018 (Bakker et al., 2016; Landschützer et al., 2020).

Appendix B: Integral time scale and variance spectra of CO_2 and vertical wind velocity

Integral time scale is used in the flux uncertainty calculation (Eq. 5 and 7). The definition of integral time scale τ_x of variable x is:

$$\tau_x = \frac{1}{\sigma_x^2}\int_0^\infty r_{xx}(t)dt \tag{B1}$$

where σ_x^2 is the variance of x and r_{xx} is the auto-covariance function of x. t is the shifting time of auto-covariance (which is different from the lag time between w and CO_2 in the EC flux calculation). We can use Eq. B1 to estimate the integral time scale of w and CO_2 directly. However, integration up to infinity is not practical. Instead we can numerically estimate the time scale by determining the time corresponding to the auto-covariance coefficient function (r_{xx}/σ_x^2) value decaying to 1/e (1/e decaying method) or by integrating the auto-covariance function up to the first zero crossing of the function (zero crossing method) (Rannik et al., 2009).

One can also use similarity theory to estimate the integral time scale theoretically (Blomquist et al., 2010):

$$\tau_w = 2.8 \frac{z}{\overline{u_r}} f_\tau(z/L) \tag{B2}$$

Here, $\overline{u_r}$ is the relative wind speed. The similarity function $f_\tau(z/L)$ is described by the stability parameter z/L where z is the observation height (m) and L is the Obukhov length (m) (Blomquist et al., 2010).

Yet another method to estimate the integral time scale is from the peak frequency (f_{max}) in the w variance spectrum (Kaimal and Finnigan, 1994):

$$\tau_w = \frac{1}{2\pi f_{max}} \tag{B3}$$

The integral time scales of w estimated by these four methods for cruise JR18007 are shown in Figure B1. The integral time scale estimated by the zero crossing method agrees well with the peak frequency estimates using Eq. B3. The 1/e decaying method tends to underestimate the integral time scale, which is generally observed for turbulent signals (Rannik et al., 2009), whereas the similarity method (Eq. B2) considerably overestimates the integral time scale. Based on the recent analysis (as yet unpublished) of the entire NOAA PSL flux database, the Eq. B2 formulation is now thought to be an overestimate (review comment for this paper from B. Blomquist, 2021). In this study we use the integral time scale of w from the zero crossing method to estimate the theoretical flux uncertainty (Eq. 5 and 7). The theoretical systematic error estimates (Eq. 8) also require the integral time scale of CO_2. The integral time scale of CO_2 is difficult to evaluate from the above four methods due to instrument noise. Instead, we estimate it by directly integrating the auto-covariance function (Eq. B1) to a shift time of 200 s (we found no significant difference of the integral time scale when integrating the CO_2 auto-covariance function for shift times ranging from 150 s to 250 s).

676
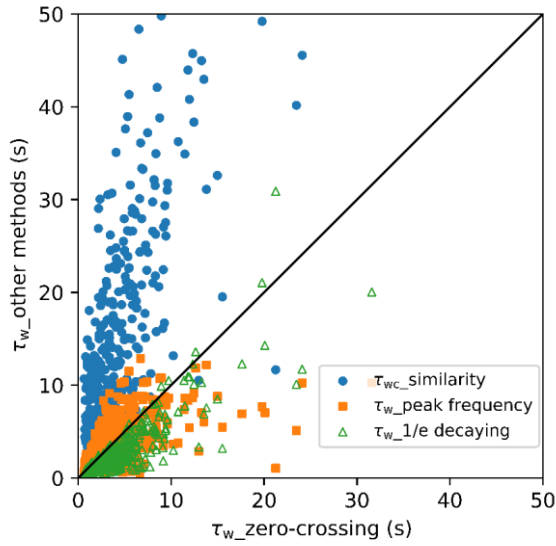
Figure B1. Comparison of integral time scales of *w* estimated by four different methods. Estimated integral time scales from the zero crossing method (integrating the auto-covariance function up to first zero crossing the function) agree well with the estimation of peak frequency method (Eq. B3). However, the similarity method (Eq. B2) overestimates the integral time scale whereas the 1/e decaying method (determining the time needed for the auto-covariance coefficient function value to decay to 1/e) tends to underestimate the integral time scale.

677
678
679
680
681
682

683

684
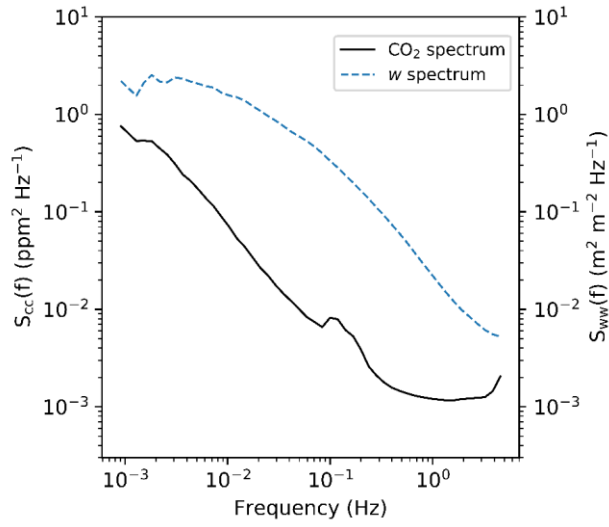
Figure B2. Mean variance spectra for CO_2 and w for one Arctic cruise JR18007. The near constant CO_2

variance at high frequency (1-5 Hz) indicates the band-limited noise in the CO_2 signal. In contrast, the

w spectrum does not show a similar band-limited noise at < 10 Hz.

688

Appendix C: Comparison of the uncertainty estimates by different methods

690
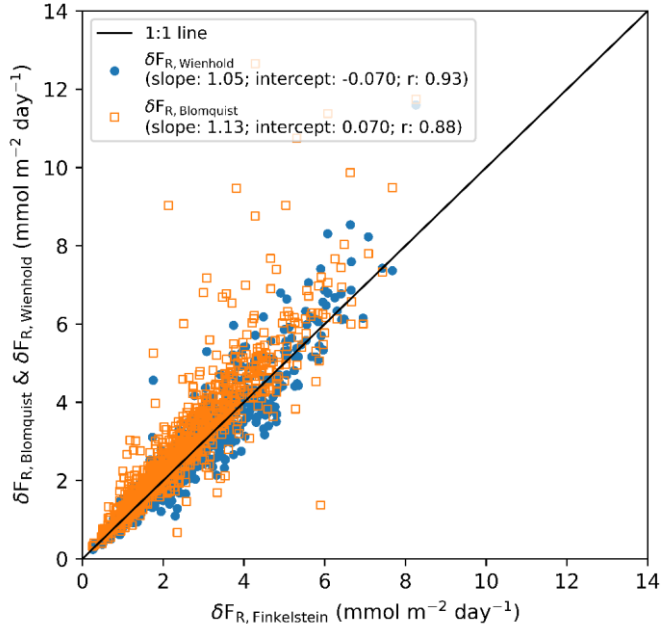
Figure C1. Comparison of total random uncertainties in hourly flux estimated by three different methods for the Arctic cruises. The empirical estimates $F_{R,\text{Wienhold}}$ agree well with one of the theoretical estimates $\Delta F_{R,\text{Finkelstein}}$ (r = 0.93). The other theoretical estimate $\Delta F_{R,\text{Blomquist}}$ is slightly higher than the random uncertainties $\Delta F_{R,\text{Finkelstein}}$ (slope = 1.13) if the constant in Eq. 8 is set equal to $\sqrt{2}$.

698
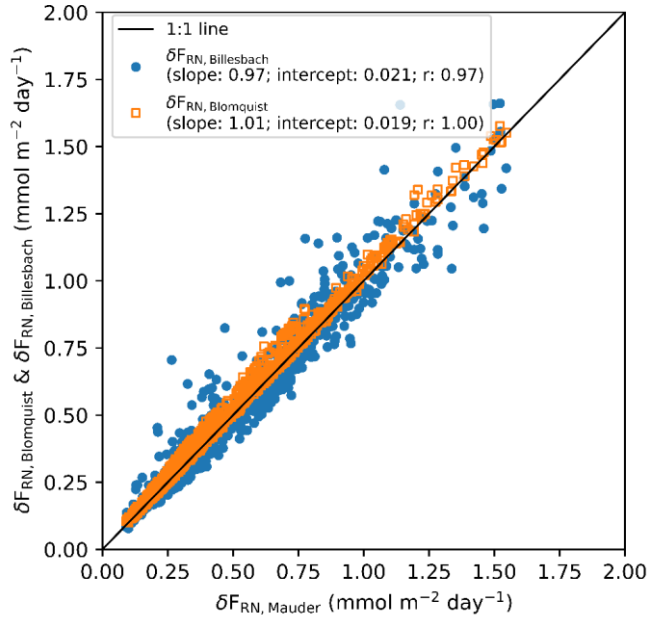
Figure C2. Comparison of random error in hourly flux due to instrument white noise, estimated by three different methods for the Arctic cruises. The three uncertainty estimations agree well. The correlation coefficient (r) between $\delta F_{RN, \text{Mauder}}$ and $\delta F_{RN, \text{Blomquist}}$ is 1 if the constant in Eq. 7 (a) is set to $\sqrt{2}$.

703

Appendix D: Performance of two gas analysers

Figure D1 shows a comparison between the performance of the Picarro 2311-f and the LI-7200 gas analysers. We estimated that the noise of the LI-7200 is on average 3 times higher than that of the Picarro 2311-f (Table 3). Indeed, random error in the CO_2 flux due to the white noise is much higher for the LI-7200 than for the Picarro 2311-f, but the total flux uncertainty of the EC system with the LI-7200 on AMT29 is only slightly higher than that of the EC system with the Picarro 2311-f on AMT28 (Table 4). Again, this is because for both EC systems, sampling error dominates the total random uncertainty, while the contribution of instrument noise (< 30%) to the total uncertainty is relatively small (Billesbach, 2011; Langford et al., 2015; Mauder et al., 2013; Rannik et al., 2016). Another often used CRDS gas analyser in EC measurements is the Los Gatos Research (LGR) Fast Greenhouse Gas Analyser (FGGA)

715 (Prytherch et al., 2017). Yang et al. (2016) showed that LGR FGGA is ca. 10 times noisier than

716 the Picarro G2311-f, and as a result the total CO_2 flux uncertainty measured by the LGR is 4

717 times higher than that by the Picarro. From the perspective of measurement noise, Picarro and

718 LI-7200 gas analysers are better suited for air-sea CO_2 flux measurements than the LGR FGGA.

719
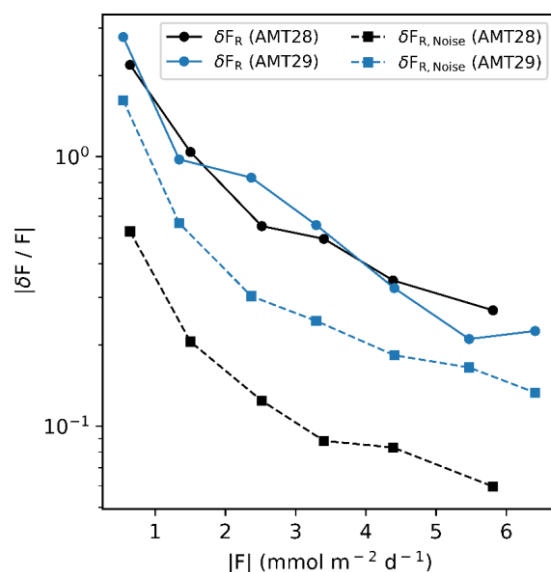
720

721 **Figure D1.** Comparison of the relative total random uncertainty and the relative random error

722 component due to white noise for different gas analysers. A Picarro G2311-f gas analyser was used on

723 AMT28 and a LI-7200 infrared gas analyser on AMT29.

724

725

726 *Data availability.* The processed hourly EC CO_2 fluxes and uncertainties can be found in the

727 Supplement of this paper. Raw, high frequency (10 Hz) data are large (tens of gigabytes) and are

728 archived at PML. Please contact the authors directly if you are interested in the raw data.

729

730 *Supplement.* The supplement related to this article is available online at:

731

Author contributions. TB and MY designed and installed the eddy covariance systems on ships and managed the collections of measurements. VK collected and processed the CO_2 fugacity data. YD processed and analysed the data with the help of MY and TB. YD wrote the paper with input from DB, TB and MY. All authors contributed to and approved the final manuscript.

Competing interests. The authors declare that they have no conflict of interest.

Acknowledgements. We thank captains and crew of the RRS James Clark Ross and RRS Discovery and all those who have helped keep the CO_2 flux systems running. We are extremely grateful to B. J. Butterworth (University of Calgary) for his advice on how to setup and run the automated CO_2 flux system on JCR and how to code the CR6 data logger, as well as to T. J. Smyth (PML) for setting up the remote monitoring of flux data. We also greatly appreciate I. Brown (PML) and D. Phillips for fCO_2 measurements and P. S. Liss (UEA) for support and helpful comments.

Financial support. This work is funded by the China Scholarship Council (CSC/201906330072). Air-sea CO_2 flux measurements were facilitated by European Space Agency (ESA AMT4oceanSatFlux project, grant no. 4000125730/18/NL/FF/gp) and support from the Natural Environment Research Council (NERC) via PML's contribution to the ORCHESTRA program (NE/N018095/1). The Arctic cruises were also supported by NERC, through the DIAPOD (NE/P006280/2) and ChAOS (NE/P006493/1) projects.

Review statement. This paper was edited by Leiming Zhang and reviewed by Byron Blomquist and an anonymous reviewer.

References

Bakker, D. C. E., Pfeil, B., Landa, C. S., Metzl, N., O'Brien, K. M., Olsen, A., Smith, K., Cosca, C., Harasawa, S., Jones, S. D., Nakaoka, S. I., Nojiri, Y., Schuster, U., Steinhoff, T., Sweeney, C., Takahashi, T., Tilbrook, B., Wada, C., Wanninkhof, R., Alin, S. R., Balestrini, C. F., Barbero, L., Bates, N. R., Bianchi, A. A., Bonou, F., Boutin, J., Bozec, Y., Burger, E. F., Cai, W. J., Castle, R. D., Chen, L., Chierici, M., Currie, K., Evans, W., Featherstone, C., Feely, R. A., Fransson, A., Goyet, C., Greenwood, N., Gregor, L., Hankin, S., Hardman-Mountford, N. J., Harlay, J., Hauck, J., Hoppema, M., Humphreys, M. P., Hunt, C. W., Huss, B., Ibánhez, J. S. P., Johannessen, T., Keeling, R., Kitidis, V., Körtzinger, A., Kozyr, A., Krasakopoulou, E., Kuwata, A., Landschützer, P., Lauvset, S. K., Lefèvre, N., Lo Monaco, C., Manke, A., Mathis, J. T., Merlivat, L., Millero, F.

J., Monteiro, P. M. S., Munro, D. R., Murata, A., Newberger, T., Omar, A. M., Ono, T., Paterson, K., Pearce, D., Pierrot, D., Robbins, L. L., Saito, S., Salisbury, J., Schlitzer, R., Schneider, B., Schweitzer, R., Sieger, R., Skjelvan, I., Sullivan, K. F., Sutherland, S. C., Sutton, A. J., Tadokoro, K., Telszewski, M., Tuma, M., Van Heuven, S. M. A. C., Vandemark, D., Ward, B., Watson, A. J. and Xu, S.: A multi-decade record of high-quality fCO_2 data in version 3 of the Surface Ocean CO_2 Atlas (SOCAT), Earth Syst. Sci. Data, 8(2), 383–413, doi:10.5194/essd-8-383-2016, 2016.

Baldocchi, D., Falge, E., Gu, L., Olson, R., Hollinger, D., Running, S., Anthoni, P., Bernhofer, C., Davis, K. and Evans, R.: FLUXNET: A new tool to study the temporal and spatial variability of ecosystem-scale carbon dioxide, water vapor, and energy flux densities, Bull. Am. Meteorol. Soc., 82(11), 2415–2434, 2001.

Bariteau, L., Helmig, D., Fairall, C. W., Hare, J. E., Hueber, J. and Lang, E. K.: Determination of oceanic ozone deposition by ship-borne eddy covariance flux measurements, Atmos. Meas. Tech., 3(2), 441–455, doi:10.5194/amt-3-441-2010, 2010.

Bell, T. G., De Bruyn, W., Marandino, C. A., Miller, S. D., Law, C. S., Smith, M. J. and Saltzman, E. S.: Dimethylsulfide gas transfer coefficients from algal blooms in the Southern Ocean, Atmos. Chem. Phys., 15(4), 1783–1794, 2015.

Billesbach, D. P.: Estimating uncertainties in individual eddy covariance flux measurements: A comparison of methods and a proposed new method, Agric. For. Meteorol., 151(3), 394–405, doi:10.1016/j.agrformet.2010.12.001, 2011.

Blomquist, B. W., Huebert, B. J., Fairall, C. W. and Faloona, I. C.: Determining the sea-air flux of dimethylsulfide by eddy correlation using mass spectrometry, Atmos. Meas. Tech., 3(1), 1–20, doi:10.5194/amt-3-1-2010, 2010.

Blomquist, B. W., Fairall, C. W., Huebert, B. J. and Wilson, S. T.: Direct measurement of the oceanic carbon monoxide flux by eddy correlation, Atmos. Meas. Tech., 5(12), 3069–3075, doi:10.5194/amt-5-3069-2012, 2012.

Blomquist, B. W., Huebert, B. J., Fairall, C. W., Bariteau, L., Edson, J. B., Hare, J. E. and McGillis, W. R.: Advances in Air-Sea CO_2 Flux Measurement by Eddy Correlation, Boundary-Layer Meteorol., 152(3), 245–276, doi:10.1007/s10546-014-9926-2, 2014.

Blomquist, B. W., Brumer, S. E., Fairall, C. W., Huebert, B. J., Zappa, C. J., Brooks, I. M., Yang, M., Bariteau, L., Prytherch, J., Hare, J. E., Czerski, H., Matei, A. and Pascal, R. W.: Wind Speed and Sea State Dependencies of Air-Sea Gas Transfer: Results From the High Wind Speed Gas Exchange Study (HiWinGS), J. Geophys. Res. Ocean., 122(10), 8034–8062, doi:10.1002/2017JC013181, 2017.

Broecker, W. S. and Peng, T. H.: Greenhouse Puzzles Part 1 Keeling's World: is CO_2 Greening the Earth, k1-k112, Columbia University, 1993.

Broecker, W. S., Ledwell, J. R., Takahashi, T., Weiss, R., Merlivat, L., Memery, L., Peng, T., Jahne, B. and Munnich, K. O.: Isotopic versus micrometeorologic ocean CO_2 fluxes: A serious conflict, J. Geophys. Res. Ocean., 91(C9), 10517–10527, 1986.

Businger, J.: Evaluation of the accuracy with which dry deposition can be measured with current micrometeorological techniques, J. Clim. Appl. Meteorol., 25(8), 1100–1124, 1986.

Butterworth, B. J. and Miller, S. D.: Air-sea exchange of carbon dioxide in the Southern Ocean and Antarctic marginal ice zone, Geophys. Res. Lett., 43(13), 7223–7230, doi:10.1002/2016GL069581, 2016.

Edson, J. B., Hinton, A. A., Prada, K. E., Hare, J. E. and Fairall, C. W.: Direct covariance flux estimates from mobile platforms at sea, J. Atmos. Ocean. Technol., 15(2), 547–562, doi:10.1175/1520-0426(1998)015<0547:DCFEFM>2.0.CO;2, 1998.

Edson, J. B., Fairall, C. W., Bariteau, L., Zappa, C. J., Cifuentes-Lorenzen, A., McGillis, W. R., Pezoa, S., Hare, J. E. and Helmig, D.: Direct covariance measurement of CO_2 gas transfer velocity during the 2008 Southern Ocean Gas Exchange Experiment: Wind speed dependency, J. Geophys. Res. Ocean., 116(11), doi:10.1029/2011JC007022, 2011.

Edson, J. B., Jampana, V., Weller, R. A., Bigorre, S. P., Plueddemann, A. J., Fairall, C. W., Miller, S. D., Mahrt, L., Vickers, D. and Hersbach, H.: On the exchange of momentum over the open ocean, J. Phys. Oceanogr., 43(8), 1589–1610, 2013.

Else, B. G. T., Papakyriakou, T. N., Galley, R. J., Drennan, W. M., Miller, L. A. and Thomas, H.: Wintertime CO_2 fluxes in an Arctic polynya using eddy covariance: Evidence for enhanced air-sea gas transfer during ice formation, J. Geophys. Res. Ocean., 116(9), doi:10.1029/2010JC006760, 2011.

Fairall, C. W., Hare, J. E., Edson, J. B. and McGillis, W.: Parameterization and micrometeorological measurement of air-sea gas transfer, Boundary-Layer Meteorol., 96(1–2), 63–105, doi:10.1023/a:1002662826020, 2000.

Finkelstein, P. L. and Sims, P. F.: Sampling error in eddy correlation flux measurements, J. Geophys. Res. Atmos., 106(D4), 3503–3509, 2001.

Flügge, M., Paskyabi, M. B., Reuder, J., Edson, J. B. and Plueddemann, A. J.: Comparison of direct covariance flux measurements from an offshore tower and a buoy, J. Atmos. Ocean. Technol., 33(5), 873–890, doi:10.1175/JTECH-D-15-0109.1, 2016.

Friedlingstein, P., O'Sullivan, M., Jones, M. W., Andrew, R. M., Hauck, J., Olsen, A., Peters, G. P., Peters, W., Pongratz, J., Sitch, S., Le Quéré, C., Canadell, J. G., Ciais, P., Jackson, R. B., Alin, S., Aragão, L. E. O. C., Arneth, A., Arora, V., Bates, N. R., Becker, M., Benoit-Cattin, A., Bittig, H. C., Bopp, L., Bultan, S., Chandra, N., Chevallier, F., Chini, L. P., Evans, W., Florentie, L., Forster, P. M., Gasser, T., Gehlen, M., Gilfillan, D., Gkritzalis, T., Gregor, L., Gruber, N., Harris, I., Hartung, K., Haverd, V., Houghton, R. A., Ilyina, T., Jain, A. K., Joetzjer, E., Kadono, K., Kato, E., Kitidis, V., Korsbakken, J. I., Landschützer, P., Lefèvre, N., Lenton, A., Lienert, S., Liu, Z., Lombardozzi, D., Marland, G., Metzl, N., Munro, D. R., Nabel, J. E. M. S., Nakaoka, S.-I., Niwa, Y., O'Brien, K., Ono, T., Palmer, P. I., Pierrot, D., Poulter, B., Resplandy, L., Robertson, E., Rödenbeck, C., Schwinger, J., Séférian, R., Skjelvan, I., Smith, A. J. P., Sutton, A. J., Tanhua, T., Tans, P. P., Tian, H., Tilbrook, B., van der Werf, G., Vuichard, N., Walker, A. P., Wanninkhof, R., Watson, A. J., Willis, D., Wiltshire, A. J., Yuan, W., Yue, X. and Zaehle, S.: Global Carbon Budget 2020, Earth Syst. Sci. Data, 12(4),

837   3269–3340, doi:10.5194/essd-12-3269-2020, 2020.

838   Garbe, C. S., Rutgersson, A., Boutin, J., De Leeuw, G., Delille, B., Fairall, C. W., Gruber, N., Hare, J., Ho, D.
839   T. and Johnson, M. T.: Transfer across the air-sea interface, in Ocean-atmosphere interactions of gases and
840   particles, pp. 55–112, Springer, Berlin, Heidelberg., 2014.

841   Ho, D. T., Law, C. S., Smith, M. J., Schlosser, P., Harvey, M. and Hill, P.: Measurements of air-sea gas
842   exchange at high wind speeds in the Southern Ocean: Implications for global parameterizations, Geophys. Res.
843   Lett., 33(16), 2006.

844   Ikawa, H., Faloona, I., Kochendorfer, J., Paw U, K. T. and Oechel, W. C.: Air-sea exchange of CO_2 at a
845   Northern California coastal site along the California Current upwelling system, Biogeosciences, 10(7), 4419–
846   4432, doi:10.5194/bg-10-4419-2013, 2013.

847   JCGM, J.: Evaluation of measurement data—Guide to the expression of uncertainty in measurement, Int. Organ.
848   Stand. Geneva ISBN, 50, 134, 2008.

849   Jones, E. P. and Smith, S. D.: A first measurement of sea-air CO_2 flux by eddy correlation, J. Geophys. Res.,
850   82(37), 5990–5992, 1977.

851   Kaimal, J. C. and Finnigan, J. J.: Atmospheric boundary layer flows: their structure and measurement, Oxford
852   university press., 1994.

853   Kaimal, J. C., Wyngaard, J. C., Izumi, Y. and Cote, O. R.: Spectral characteristics of surface-layer turbulence,
854   Q. J. R. Meteorol. Soc., 098(417), 563–589, doi:10.1256/smsqj.41706, 1972.

855   Kohsiek, W.: Water vapor cross-sensitivy of open path H_2O/CO_2 sensors, J. Atmos. Ocean. Technol., 17(3),
856   299–311, doi:10.1175/1520-0426(2000)017<0299:WVCSOO>2.0.CO;2, 2000.

857   Kondo, F. and Tsukamoto, O.: Air-sea CO_2 flux by eddy covariance technique in the equatorial Indian Ocean, J.
858   Oceanogr., 63(3), 449–456, doi:10.1007/s10872-007-0040-7, 2007.

859   Landschützer, P., Gruber, N. and Bakker, D. C. E.: An observation-based global monthly gridded sea surface
860   pCO_2 product from 1982 onward and its monthly climatology (NCEI Accession 0160558), Version 5.5, NOAA
861   National Centers for Environmental Information, Dataset, https://doi.org/10.7289/V5Z899N6, 2020.

862   Landwehr, S., Miller, S. D., Smith, M. J., Saltzman, E. S. and Ward, B.: Analysis of the PKT correction for
863   direct CO_2 flux measurements over the ocean, Atmos. Chem. Phys., 14(7), 3361–3372, doi:10.5194/acp-14-
864   3361-2014, 2014.

865   Landwehr, S., Miller, S. D., Smith, M. J., Bell, T. G., Saltzman, E. S. and Ward, B.: Using eddy covariance to
866   measure the dependence of air-sea CO2 exchange rate on friction velocity, Atmos. Chem. Phys., 18(6), 4297–
867   4315, doi:10.5194/acp-18-4297-2018, 2018.

868   Langford, B., Acton, W., Ammann, C., Valach, A. and Nemitz, E.: Eddy-covariance data with low signal-to-
869   noise ratio: Time-lag determination, uncertainties and limit of detection, Atmos. Meas. Tech., 8(10), 4197–4213,
870   doi:10.5194/amt-8-4197-2015, 2015.

871 Lauvset, S. K., McGillis, W. R., Bariteau, L., Fairall, C. W., Johannessen, T., Olsen, A. and Zappa, C. J.: Direct

872 measurements of CO_2 flux in the Greenland Sea, Geophys. Res. Lett., 38(12), 2011.

873 Lenschow, D. H. and Kristensen, L.: Uncorrelated noise in turbulence measurements, J. Atmos. Ocean.

874 Technol., 2(1), 68–81, 1985.

875 Lenschow, D. H., Mann, J. and Kristensen, L.: How long is long enough when measuring fluxes and other

876 turbulence statistics? NCAR Tech. Note, NCAR/TN-389, 53 Natl. Cent. for Atmos. Res., Boulder, Colo., 1993.

877 Lenschow, D. H., Mann, J. and Kristensen, L.: How long is long enough when measuring fluxes and other

878 turbulence statistics? J. Atmos. Ocean. Technol., 11(3), 661–673, doi:10.1175/1520-

879 0426(1994)011<0661:HLILEW>2.0.CO;2, 1994.

880 Lenschow, D. H., Wulfmeyer, V. and Senff, C.: Measuring second- through fourth-order moments in noisy data,

881 J. Atmos. Ocean. Technol., 17(10), 1330–1347, doi:10.1175/1520-0426(2000)017<1330:MSTFOM>2.0.CO;2,

882 2000.

883 Loescher, H. W., Law, B. E., Mahrt, L., Hollinger, D. Y., Campbell, J. and Wofsy, S. C.: Uncertainties in, and

884 interpretation of, carbon flux estimates using the eddy covariance technique, J. Geophys. Res. Atmos., 111(21),

885 1–19, doi:10.1029/2005JD006932, 2006.

886 Mahrt, L.: Flux sampling errors for aircraft and towers, J. Atmos. Ocean. Technol., 15(2), 416–429,

887 doi:10.1175/1520-0426(1998)015<0416:FSEFAA>2.0.CO;2, 1998.

888 Mauder, M., Cuntz, M., Drüe, C., Graf, A., Rebmann, C., Schmid, H. P., Schmidt, M. and Steinbrecher, R.: A

889 strategy for quality and uncertainty assessment of long-term eddy-covariance measurements, Agric. For.

890 Meteorol., 169, 122–135, doi:10.1016/j.agrformet.2012.09.006, 2013.

891 McGillis, W. R., Edson, J. B., Ware, J. D., Dacey, J. W. H., Hare, J. E., Fairall, C. W. and Wanninkhof, R.:

892 Carbon dioxide flux techniques performed during GasEx-98, Mar. Chem., 75(4), 267–280, doi:10.1016/S0304-

893 4203(01)00042-1, 2001.

894 McGillis, W. R., Edson, J. B., Zappa, C. J., Ware, J. D., McKenna, S. P., Terray, E. A., Hare, J. E., Fairall, C.

895 W., Drennan, W. and Donelan, M.: Air-sea CO_2 exchange in the equatorial Pacific, J. Geophys. Res. Ocean.,

896 109(C8), 2004.

897 Miller, S. D., Marandino, C. and Saltzman, E. S.: Ship-based measurement of air-sea CO_2 exchange by eddy

898 covariance, J. Geophys. Res. Atmos., 115(D2), 1–14, doi:10.1029/2009JD012193, 2010.

899 Moat, B. and Yelland, M.: Airflow distortion at instrument sites on the RRS James Clark Ross during the

900 WAGES project, No. 12, National Oceanography Centre Internal Document, National Oceanography Centre,

901 Southampton, 2015.

902 Moat, B. I., Yelland, M. J. and Cooper, E. B.: The airflow distortion at instruments sites on the RRS" James

903 Cook", National Oceanography Centre Southampton Research and Consultancy Report 11, National

904 Oceanography Centre, Southampton, 44pp, 2006.

Nightingale, P. D., Malin, G., Law, C. S., Watson, A. J., Liss, P. S., Liddicoat, M. I., Boutin, J. and Upstill-Goddard, R. C.: In situ evaluation of air-sea gas exchange parameterizations using novel conservative and volatile tracers, Global Biogeochem. Cycles, 14(1), 373–387, doi:10.1029/1999GB900091, 2000.

Nilsson, E., Bergström, H., Rutgersson, A., Podgrajsek, E., Wallin, M. B., Bergström, G., Dellwik, E., Landwehr, S. and Ward, B.: Evaluating humidity and sea salt disturbances on CO_2 flux measurements, J. Atmos. Ocean. Technol., 35(4), 859–875, doi:10.1175/JTECH-D-17-0072.1, 2018.

Post, H., Hendricks Franssen, H. J., Graf, A., Schmidt, M. and Vereecken, H.: Uncertainty analysis of eddy covariance CO_2 flux measurements for different EC tower distances using an extended two-tower approach, Biogeosciences, 12(4), 1205–1221, doi:10.5194/bg-12-1205-2015, 2015.

Prytherch, J., Yelland, M. J., Pascal, R. W., Moat, B. I., Skjelvan, I. and Neill, C. C.: Direct measurements of the CO_2 flux over the ocean: Development of a novel method, Geophys. Res. Lett., 37(3), doi:10.1029/2009GL041482, 2010.

Prytherch, J., Brooks, I. M., Crill, P. M., Thornton, B. F., Salisbury, D. J., Tjernström, M., Anderson, L. G., Geibel, M. C. and Humborg, C.: Direct determination of the air-sea CO_2 gas transfer velocity in Arctic sea ice regions, Geophys. Res. Lett., 44(8), 3770–3778, 2017.

Rannik, Ü., Mammarella, I., Aalto, P., Keronen, P., Vesala, T. and Kulmala, M.: Long-term aerosol particle flux observations part I: Uncertainties and time-average statistics, Atmos. Environ., 43(21), 3431–3439, doi:10.1016/j.atmosenv.2009.02.049, 2009.

Rannik, Ü., Peltola, O. and Mammarella, I.: Random uncertainties of flux measurements by the eddy covariance technique, Atmos. Meas. Tech., 9(10), 5163–5181, doi:10.5194/amt-9-5163-2016, 2016.

Smith, S. D. and Jones, E. P.: Evidence for wind-pumping of air-sea gas exchange based on direct measurements of CO_2 fluxes, J. Geophys. Res. Ocean., 90(C1), 869–875, 1985.

Spreen, G., Kaleschke, L. and Heygster, G.: Sea ice remote sensing using AMSR-E 89-GHz channels, J. Geophys. Res. Ocean., 113(C2), doi:10.1029/2005JC003384, 2008.

Takahashi, T., Sutherland, S. C., Wanninkhof, R., Sweeney, C., Feely, R. A., Chipman, D. W., Hales, B., Friederich, G., Chavez, F., Sabine, C., Watson, A., Bakker, D. C. E., Schuster, U., Yoshikawa-Inoue, H., Ishii, M., Midorikawa, T., Nojiri, Y., Körtzinger, A., Steinhoff, T., Hoppema, M., Olafsson, J., Arnarson, T. S., Johannessen, T., Olsen, A., Bellerby, R., Wong, C. S., Delille, B., Bates, N. R. and de Baar, H. J. W.: Climatological mean and decadal change in surface ocean pCO2, and net sea–air CO_2 flux over the global oceans, Deep Sea Res. Part II Top. Stud. Oceanogr., 56(8–10), 554–577, doi:10.1016/J.DSR2.2008.12.009, 2009.

Tsukamoto, O., Kondo, F. and Kamei, Y.: Overestimation of downward air-sea eddy CO_2 flux due to optical window contamination of open-path gas analyzer, SOLA, 10, 117–121, 2014.

Wanninkhof, R.: Relationship between wind speed and gas exchange over the ocean revisited, Limnol. Oceanogr. Methods, 12(6), 351–362, doi:10.4319/lom.2014.12.351, 2014.

940 Weiss, A., Kuss, J., Peters, G. and Schneider, B.: Evaluating transfer velocity-wind speed relationship using a
941 long-term series of direct eddy correlation CO_2 flux measurements, J. Mar. Syst., 66(1–4), 130–139,
942 doi:10.1016/j.jmarsys.2006.04.011, 2007.

943 Wesely, M. L., Cook, D. R., Hart, R. L. and Williams, R. M.: Air-sea exchange of CO_2 and evidence for
944 enhanced upward fluxes, J. Geophys. Res. Ocean., 87(C11), 8827–8832, 1982.

945 Wienhold, F. G., Welling, M. and Harris, G. W.: Micrometeorological measurement and source region analysis
946 of nitrous oxide fluxes from an agricultural soil, Atmos. Environ., 29(17), 2219–2227, 1995.

947 Woolf, D. K., Shutler, J. D., Goddijn-Murphy, L., Watson, A. J., Chapron, B., Nightingale, P. D., Donlon, C. J.,
948 Piskozub, J., Yelland, M. J., Ashton, I., Holding, T., Schuster, U., Girard-Ardhuin, F., Grouazel, A., Piolle, J. F.,
949 Warren, M., Wrobel-Niedzwiecka, I., Land, P. E., Torres, R., Prytherch, J., Moat, B., Hanafin, J., Ardhuin, F.
950 and Paul, F.: Key uncertainties in the recent air-sea flux of CO_2, Global Biogeochem. Cycles, 33(12), 1548–
951 1563, doi:10.1029/2018GB006041, 2019.

952 Wyngaard, J. C.: Turbulence in the Atmosphere Part 1, Chapt. 2, Getting to know turbulence, p27-54
953 Cambridge University Press., 2010.

954 Yang, M., Nightingale, P. D., Beale, R., Liss, P. S., Blomquist, B. and Fairall, C.: Atmospheric deposition of
955 methanol over the Atlantic Ocean, Proc. Natl. Acad. Sci. U. S. A., 110(50), 20034–20039,
956 doi:10.1073/pnas.1317840110, 2013.

957 Yang, M., Prytherch, J., Kozlova, E., Yelland, M. J., Parenkat Mony, D. and Bell, T. G.: Comparison of two
958 closed-path cavity-based spectrometers for measuring air-water CO_2 and CH_4 fluxes by eddy covariance,
959 Atmos. Meas. Tech., 9(11), 5509–5522, doi:10.5194/amt-9-5509-2016, 2016.

960 Yelland, M. J., Moat, B. I., Taylor, P. K., Pascal, R. W., Hutchings, J. and Cornell, V. C.: Wind stress
961 measurements from the open ocean corrected for airflow distortion by the ship, J. Phys. Oceanogr., 28(7), 1511–
962 1526, doi:10.1175/1520-0485(1998)028<1511:WSMFTO>2.0.CO;2, 1998.

963

964